Supplemental Data

A

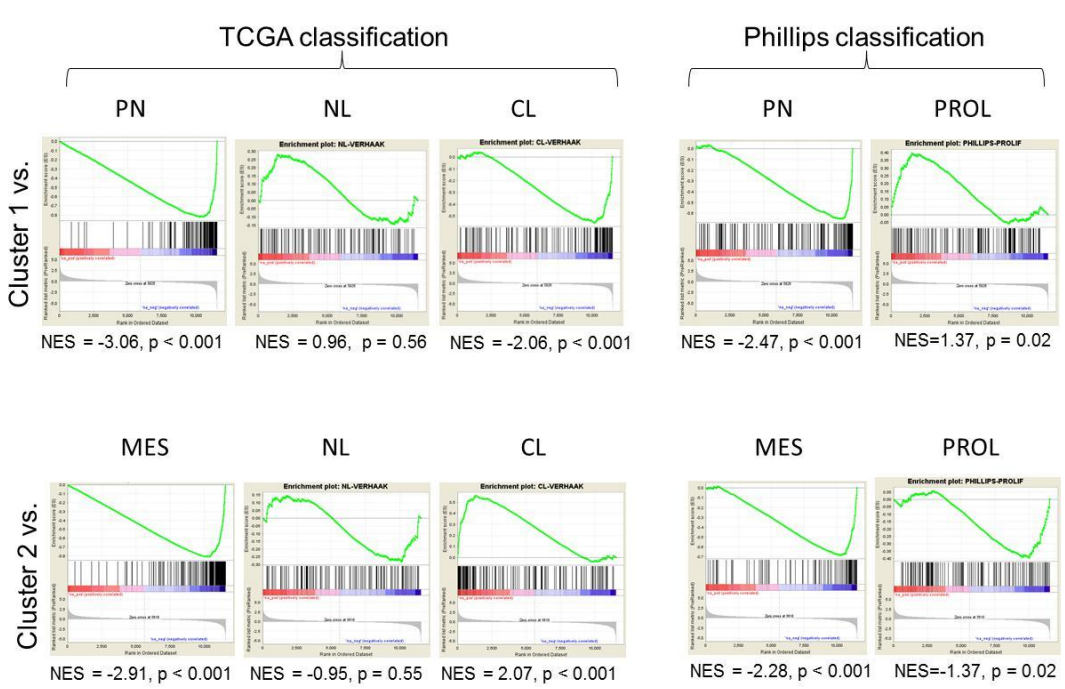

B

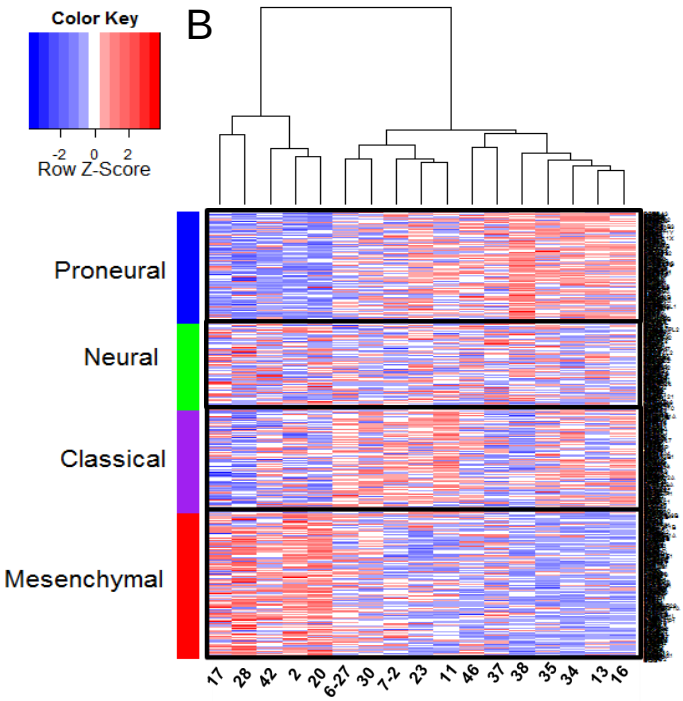

C

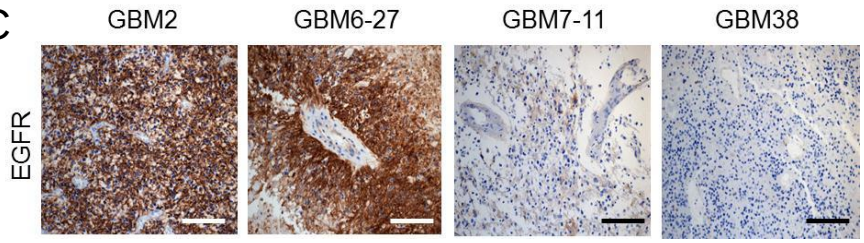

EGFR

Sample ID	GSC (DNA copy number)	GBM (IHC)
13	normal	-
11	amp(~4 copies)	+++
17	normal	-
34	amp (~14 copies)	+++
2	amp (~6 copies)	+++
16	normal	-
7-11	normal	-
7-2	normal	-
30	amp (~4 copies)	+++
6-27	normal	+++
38	normal	-
20	amp (~4 copies)	ND
28	normal	-
267	normal	-

"-" no detectable level
"+++" high expression
"ND" not determined

D

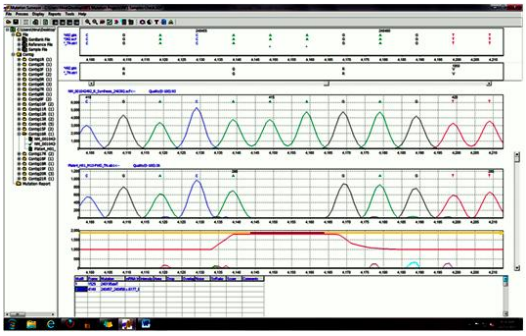

GSC 6-27, EX 39:
Homozygous 2bp deletion of AA (240457_240458)

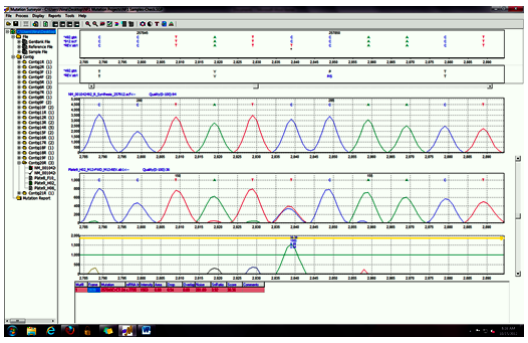

GSC 28, EX 50:
(257849C>CT : 2488P>P/S)

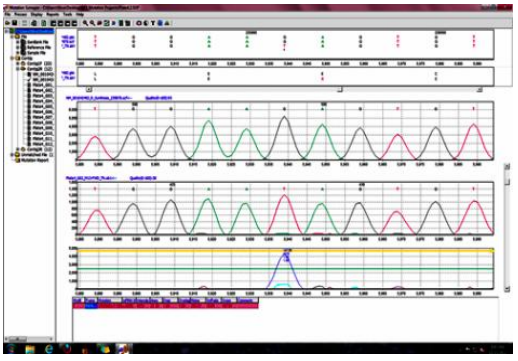

GSC 28, EX 38
(235996G>T : 1908E>X)

PN GSC
MES GSC

E

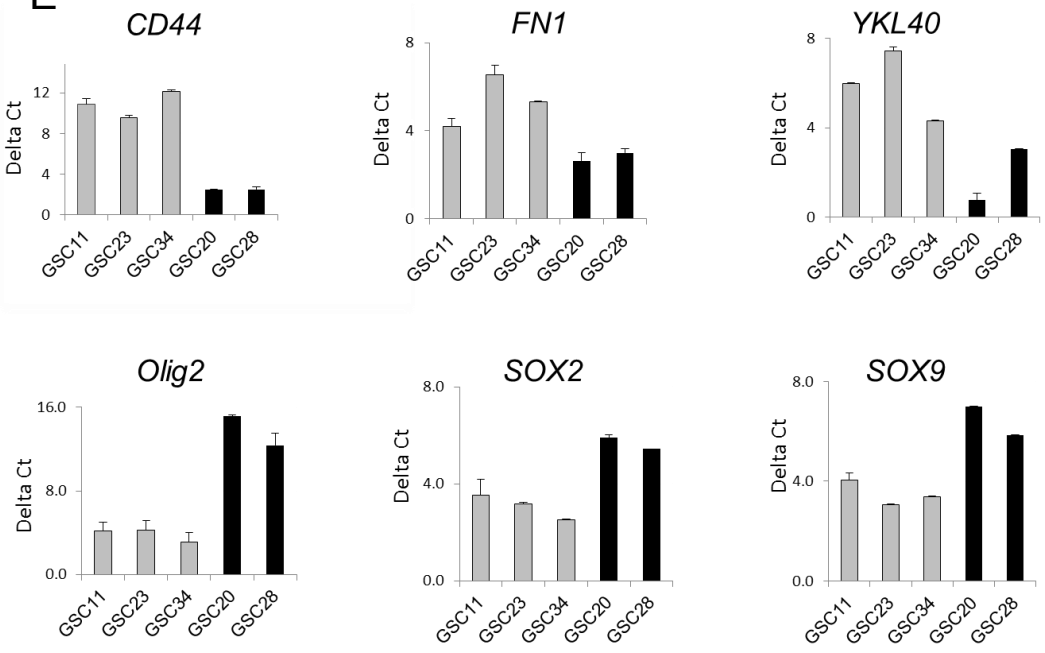

F

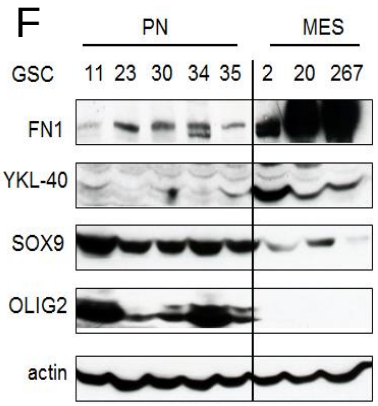

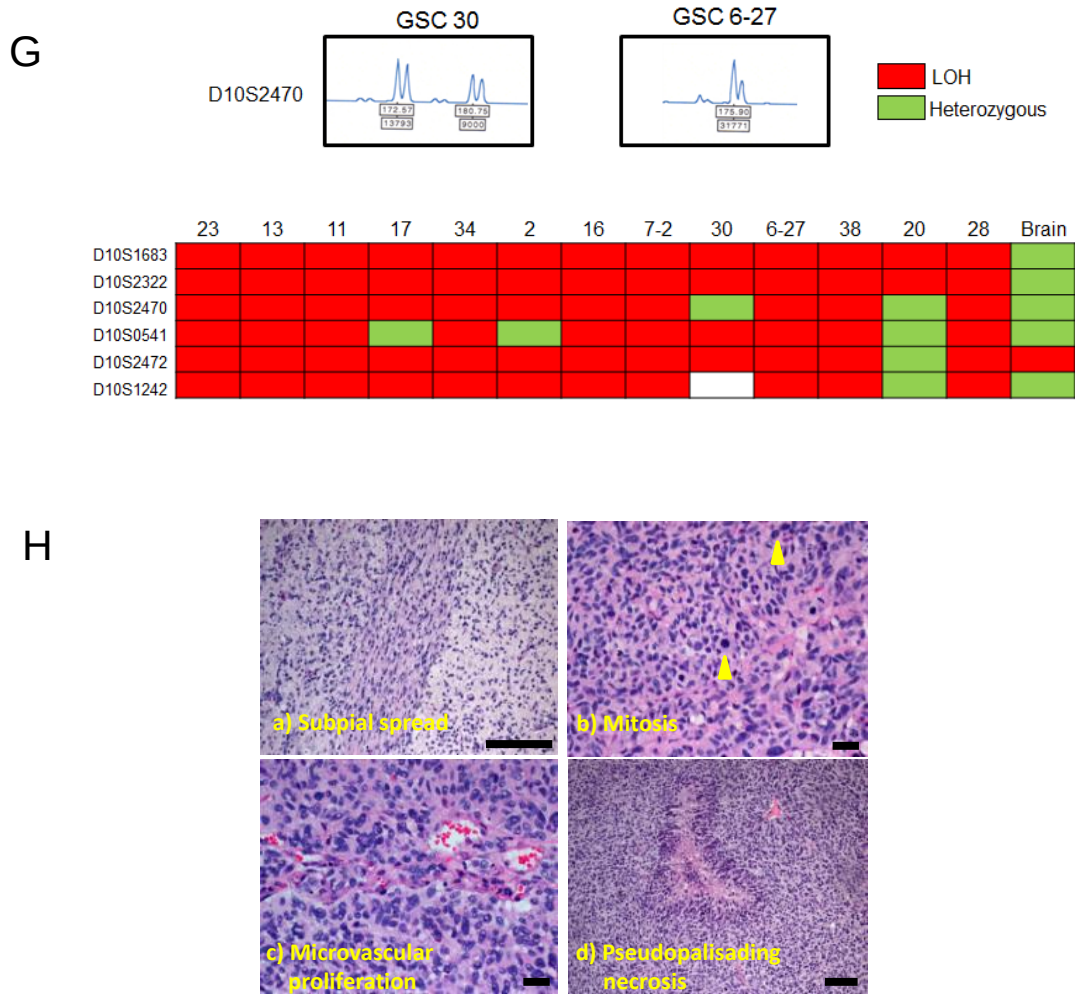

Figure S1, related to Figure 1.

(A) GSEA of genes specifically enriched either in cluster 1 or 2. A ranked gene list of cluster genes on HGU133a version 2 microarray chip was compared against PN, MES, NL, CL or PROL gene lists defined previously (Phillips et al., 2006; Verhaak et al., 2010).

(B) Supervised hierarchical clustering of GSCs according to previously defined PN, MES, CL, or Neural (NL) subtypes (Verhaak et al., 2010).

(C) IHC staining of EGFR in GBMs is shown. Intense membrane staining is seen in tumors that have amplification versus those that do not. Scale bar: 100 μm. Bottom table shows the EGFR copy number as detected by Taqman assay. The MES GSCs are shown in red font.

(D) Sanger sequence trace showing 2 bp deletion in exon 39 of GSC 6-27 and homozygous mutations in exon 50 and exon 38 of GSC28.

(E) qRT-PCR analysis of *OLIG2, SOX2, SOX9, FN1, CD44* and *YKL40* in MES (GSC 20 and 28) and PN (GSC 11, 23 and 34) GSCs. Bar graph shows average delta Ct against *RPS27* used as a control. Note that higher delta Ct value implies lower overall gene expression. Error bar indicates +/- SD.

(F) Western blot analysis of OLIG2, SOX9, FN1, YKL-40 and actin expression in PN (11, 23, 30, 34, 35) and MES (2, 20, 267) GSCs.

(G) Representative traces of genescan for chromosome 10 are shown on top. The heatmap below shows if a call was made as LOH (red) or heterozygous (green) based on the traces.

(H) Representative hematoxylin and eosin staining of xenograft tumors derived from GSCs. Hematoxylin and eosin stains showing pathological features characteristic of GBM. (a) sub-pial spread, (b) mitotic figures (arrows), (c) microvascular proliferation, and (d) pseudopalisading necrosis. Scale bars: a & d, 100 μm; b & c, 20 μm.

Table S1 related to Figure 1. Characteristics of GBMs used to isolate GSCs

GSC	Tumor type	Clinical Status	Neurospheres (+/-)
2	GBM	primary	+
2-14	GBM	primary	+
3	GBM	primary	-
6-27	GBM	primary	+
7-2	GBM	primary (prior surgery)	+
7-6	GBM	primary	+
7-11	GBM	primary	+
11	GBM	recurrent	+
13	GBM	primary	+
14	GBM	primary	-
16	GBM	recurrent	+
17	GBM	recurrent	+
20	GBM/gliosarcoma	primary	+
21	GBM	primary	-
22	GBM	primary	-
23	GBM	recurrent	+
28	GBM/gliosarcoma	recurrent	+
30	GBM	primary	+
33	GBM	primary	-
34	GBM	recurrent	+
35	GBM	primary	+
36	GBM	primary	-
37	GBM	primary	+
38	GBM	primary	+
41	GBM	primary	-
42	GBM	primary	+
46	GBM	primary	-
48	GBM	primary	+
240	GBM	primary (prior surgery)	+
248	GBM	primary	+
262	GBM	primary	+
264	GBM	primary (prior surgery)	+
267	GBM	recurrent	+
274	GBM	recurrent	+
275	GBM	recurrent	+
280	GBM	primary	+
282	GBM	recurrent	+
283	GBM	primary	+
295	GBM	recurrent	+
296	GBM	primary	+
300	GBM	primary	+

The neurosphere forming ability of various human GBM tumors is shown. “+” indicates ability to form secondary neurospheres and subsequent propagation, and a “-” indicates inability to form secondary neurospheres and expansion.

Table S3 related to Figure 1. List of genes used as PN or MES markers in GSCs

Gene	Expression	References
YKL40	Chondrocytes, macrophages,fibroblasts, vascular smooth muscle cells etc	(Hakala et al., 1993)
		(Lee et al., 2009)
CD44	Mesenchymal progenitor cells, reactive astrocytes, multiple cancers	(Campagnoli et al., 2001; Ghilzon et al., 1999; Girgrah et al., 1991a; Girgrah et al., 1991b; Kuppner et al., 1992; Sun et al., 2003; Zohar et al., 1998)
CTGF	Endothelial cells, fibrosis, fibroblasts	(Haudenschild et al., 2001)
		(Abreu et al., 2002; Leask, 2004; Nakanishi et al., 2000)
TIMP1	Liver fibrosis, multiple scelerosis, breast carcinoma	(Bommarito et al., 2011; Kuvaja et al., 2012; Mayrand et al., 2012; Ostanin et al., 2011)
TGFBI	Cartilage, chondrocytes	(Hashimoto et al., 1997; Ohno et al., 2012)
SERPINE1	Renal fibrosis, liver fibrosis	(Bergheim et al., 2006; Narumoto et al., 2012; Samarakoon et al., [illegible]
FN1	Fibroblasts, mesoderm, vasculature	(Mao and Schwarzbauer, 2005; Mosher, 1984; Stenman and Vaheri, 1978)
OLIG2	Mature oligodendrocytes,	(Lu et al., 2002; Lu et al., 2000; Takebayashi et al., 2002; Zhou
	Oligodendrocyte precursors (OPCs)	
CD15	Neural stem cells, Glioma stem cells, Medulloblastoma stem like cells	(Capela and Temple, 2002; Hennen et al., 2011; Pruszak et al., 2009; Read et al., 2009; Son et al., 2009; Yuan et al., 2011)
SOX9	Neural stem cells, neural crest	(Cheng et al., 2009; Cheung and Briscoe., 2003; Kang et al., 2012; Scott et al., 2010; Stolt et al., 2003; Stolt et al., 2002; Wegner and Stolt, 2005)
SOX2	Neural stem cells, ES cells	(D'Amour and Gage, 2003; Favaro et al., 2009; Taranova et al., 2006)
NCAM1	Neural tube, Neural progenitor cells	(Bally-Cuif et al., 1993; Mayer-Proschel et al., 1997; Pennartz et al., 2004; Thiery et al., 1982)
ASCL1	oligodendrocyte precursor cells (OPCs),Neural progenitor cells	(Caiazzo et al., 2011; Parras et al., 2007; Ross et al., 2003; Ueno et al., 2012)
DLL3	Developing nervous system, neural progenitor cells	(Casarosa et al., 1999; Kusumi et al., 2001; Kusumi et al., 2004; Yoon and Gaiano, 2005; Zhao et al., 2009)

Genes highlighted in red represent MES whereas genes highlighted in green represent PN markers. The expression of these markers in normal tissues is indicated and referenced.

Table S4 related to Figure 1. Tumor forming capacity of GSCs

GSC	No. of cells implanted	Tumorigenic	No. of mice	Median Survival
2	500,000	yes	5/5	~ 60 days (NOD-SCID)/ ~120 days (Foxn1^{nu})
2-14	500,000	no	0/5	
6-27	500,000	yes	5/5	~90 days
6-27	100,000	yes	5/5	~90 days
7-2	500,000	yes	5/5	~60 days
7-2	100,000	yes	5/5	~60 days
7-2	10,000	yes	5/5	~90 days
7-6	500,000	no	0/5	
7-10	500,000	yes	5/5 (2/5 extracranial tumors)	~70 days (Foxn1^{nu})
7-11	500,000	yes	5/5	35 days (Foxn1^{nu})
11	500,000	yes	5/5	~ 45 days (NOD-SCID / Foxn1^{nu})
11	100,000	yes	8/8	~60 days (Foxn1^{nu})
13	500,000	yes	5/5	~ 90 days
16	500,000	no	0/5	
17	500,000	yes	5/5	~ 20 days
20	500,000	yes	5/5	~ 90 days (NOD-SCID) / ~120 days (Foxn1^{nu})
23	500,000	yes	5/5	~70 days (NOD-SCID /Foxn1^{nu})
23	100,000	yes	10/10	~ 110 days (Foxn1^{nu})
23	10,000	yes	10/10	~ 175 days (Foxn1^{nu})
25	500,000	no	0/5	
28	500,000	yes	5/5	~ 90 days (NOD-SCID) / ~120 days (Foxn1^{nu})
34	500,000	yes	5/5 (extracranial tumors)	~ 120 days (Foxn1^{nu})
38	500,000	yes	5/5	~60 days (Foxn1^{nu})

Table shows the number of cells implanted in each GSC, the number of mice forming tumors and the median survival of these animals. Note that in some cases both NOD-SCID as well as Foxn1^{nu} mice were implanted with GSCs.

Table S5 related to Figure 1. Pathological features of GSC derived tumors

GSC	PN/MES	Invasion	MVP	PPN
7-2	PN	+	+	-
11	PN	+/-	+/-	+
13	PN	+	-	+/-
23	PN	+	+/-	-
38	PN	+	-	-
17	MES	-	-	+
2	MES	+	+/-	-
20	MES	+	+	+
+/- indicates a subset of the tumors did not show these features				
MVP = microvascular proliferation				
PPN = pseudopalisading necrosis				

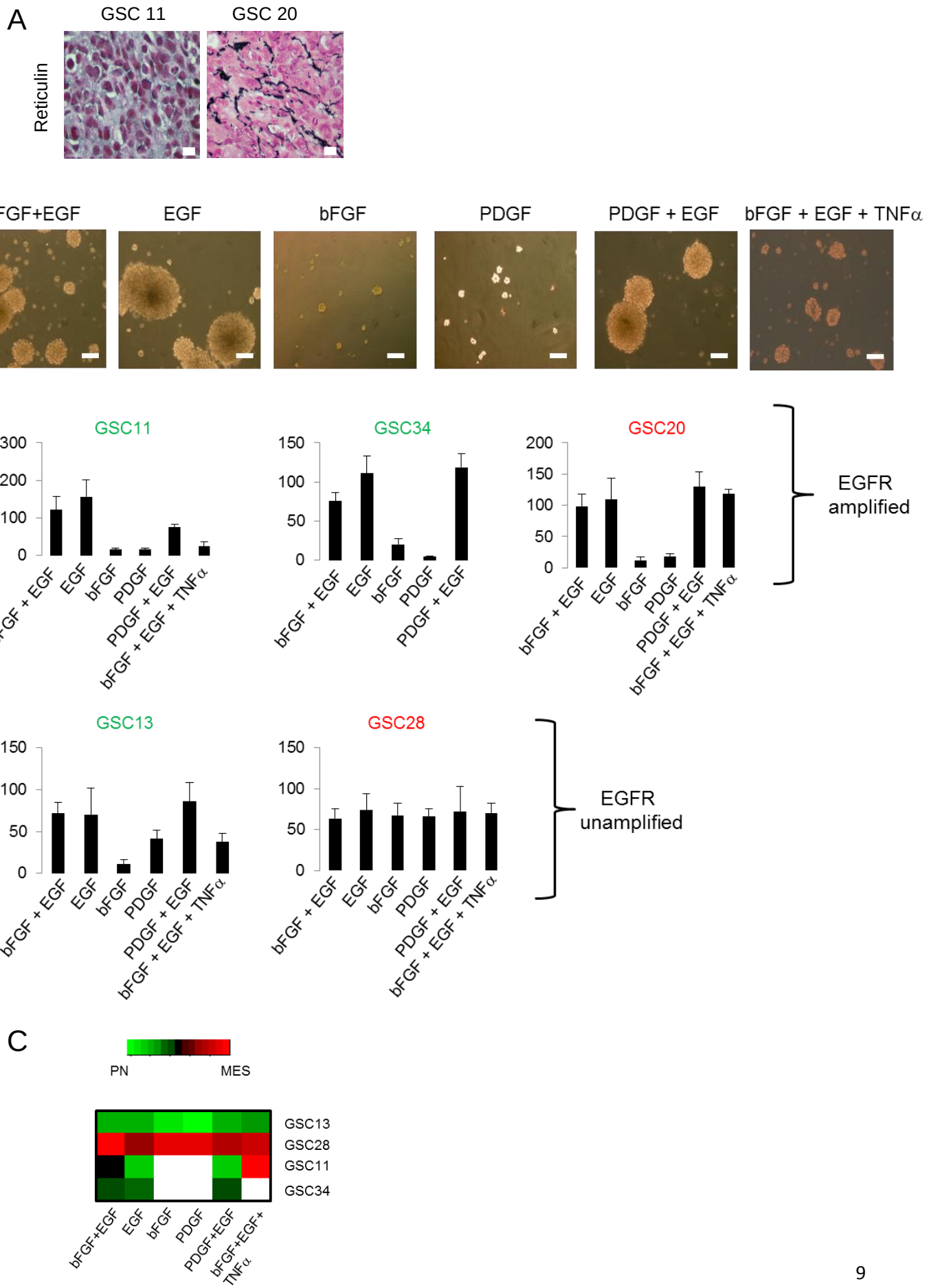
A
GSC 11
GSC 20
Reticulin
B
bFGF+EGF
EGF
bFGF
PDGF
PDGF + EGF
bFGF + EGF + TNFα
GSC11
GSC11
GSC34
GSC20
Neurospheres/field
300
200
100
0
150
100
50
0
200
150
100
50
0
bFGF + EGF
EGF
bFGF
PDGF
PDGF + EGF
bFGF + EGF + TNFα
EGFR amplified
GSC13
GSC28
EGFR unamplified
C
PN
MES
GSC13
GSC28
GSC11
GSC34
bFGF+EGF
EGF
bFGF
PDGF
PDGF+EGF
bFGF+EGF+ TNFα

D

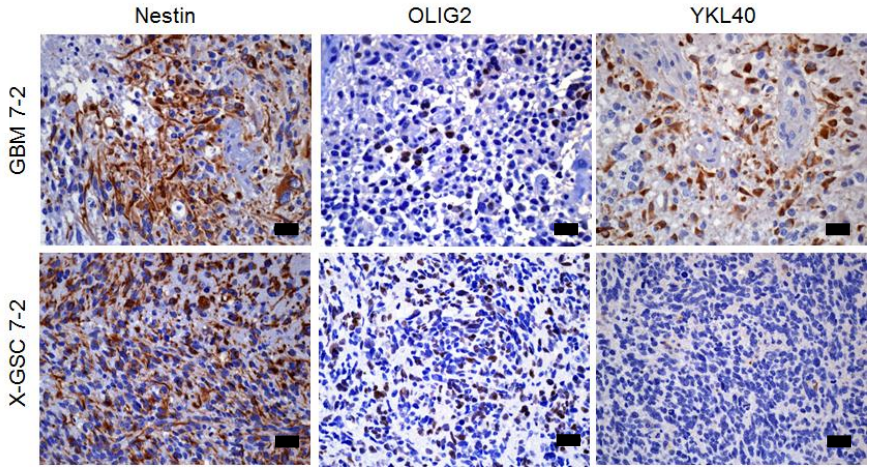
Nestin
OLIG2
YKL40
GBM 7-2
X-GSC 7-2

E

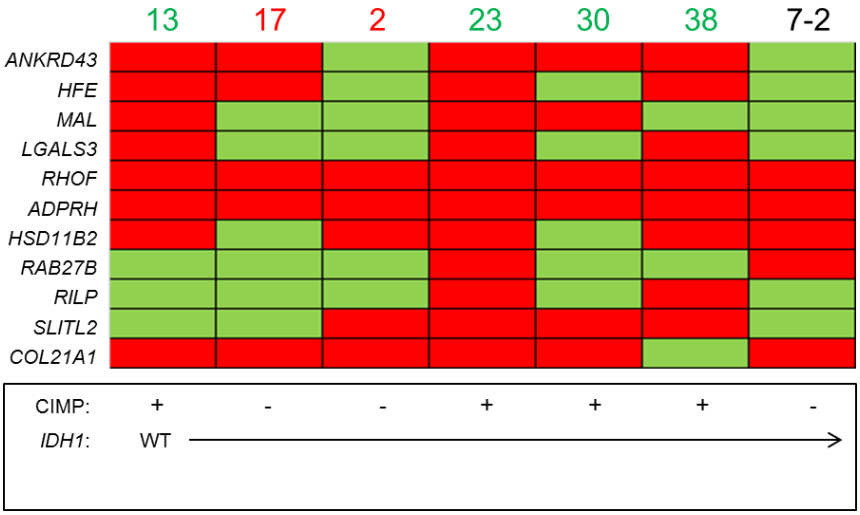
13
17
2
23
30
38
7-2
ANKRD43
HFE
MAL
LGALS3
RHOF
ADPRH
HSD11B2
RAB27B
RILP
SLITL2
COL21A1
CIMP: + - - + + + -
IDH1: WT

F

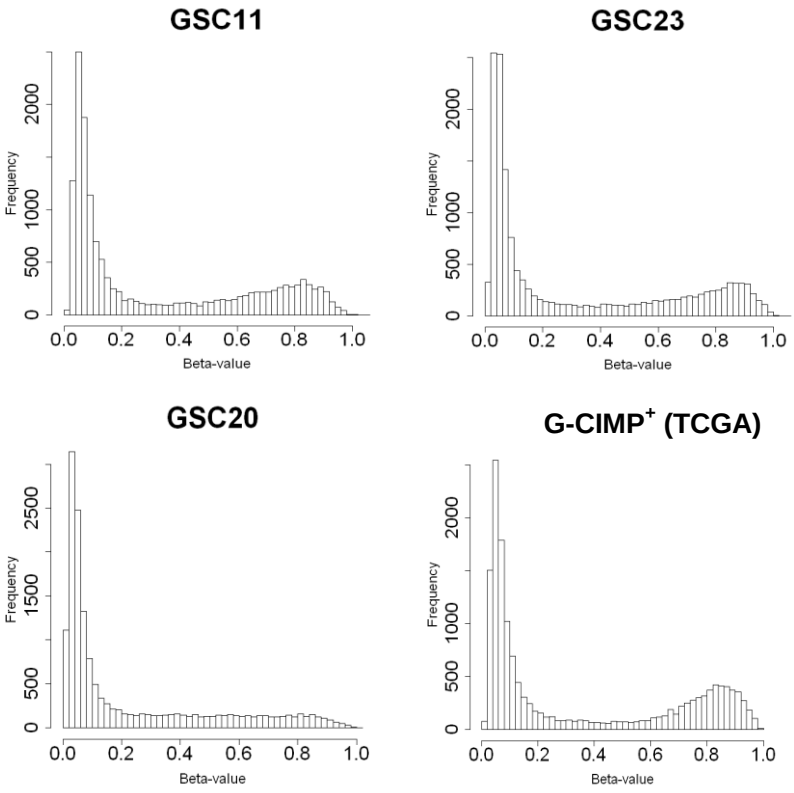
GSC11
GSC23
GSC20
G-CIMP+ (TCGA)
Frequency
Beta-value

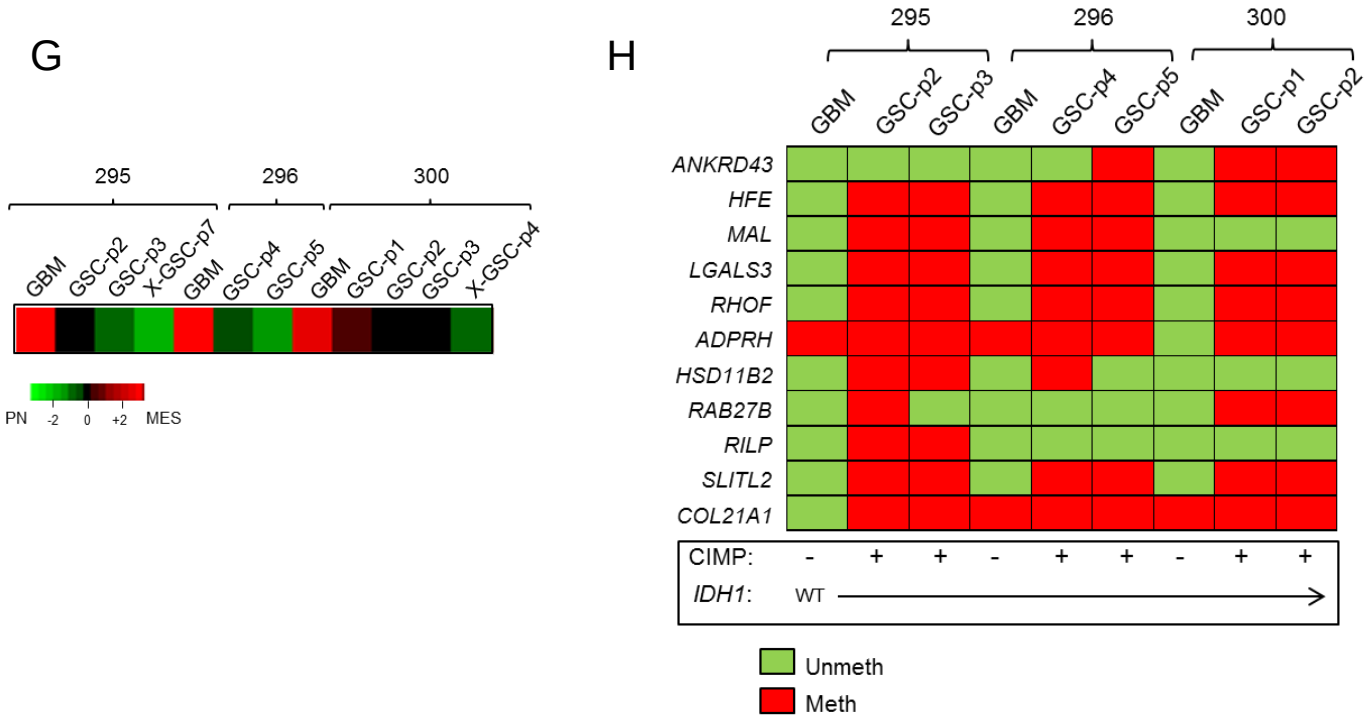

Figure S2, related to Figure 2.

(A) Reticulin staining of GSC11 and GSC20 -derived xenograft tumors. Scale bar: 20 μm.

(B) Images of GSC11 neurospheres under various growth conditions are shown on top. Scale bar: 100 μM. GSCs were cultured with differing combination of growth factors as indicated for three weeks. Bar graphs indicate mean values of number of neurospheres in three independent fields. Error bar indicates +/- SD. PN GSCs are shown with green font whereas MES GSCs are shown in red.

(C) The PN-MES metagene heatmap of GSCs cultured under varying growth factors.

(D) IHC analysis of Nestin, OLIG2 and YKL40 expression in patient matched GBM and xenografts of GSC7-2. Scale bar: 100μm.

(E) Methylight profiling of GSCs for G-CIMP status. Eleven markers were tested for presence of methylation on their promoters and coded as red if methylated and green if unmethylated. Samples were inferred as G-CIMP$^+$ if >50% of the loci showed methylation. The *IDH1* and PN/MES status of the same samples are indicated below.

(F) The histograms of GSC 11 and 23 indicate their relative global hypo/hypermethylation compared to GSC 20 and a sample G-CIMP$^+$ TCGA tumor. The bars indicate frequency of methylation after binning for β-values.

(G) Heatmap showing the predominant PN/MES gene expression signature of initiating GBM, and derived early passage GSCs.

(H) Methylight profiling of initiating GBM, and derived early passage GSCs. CIMP and *IDH1* status is shown below.

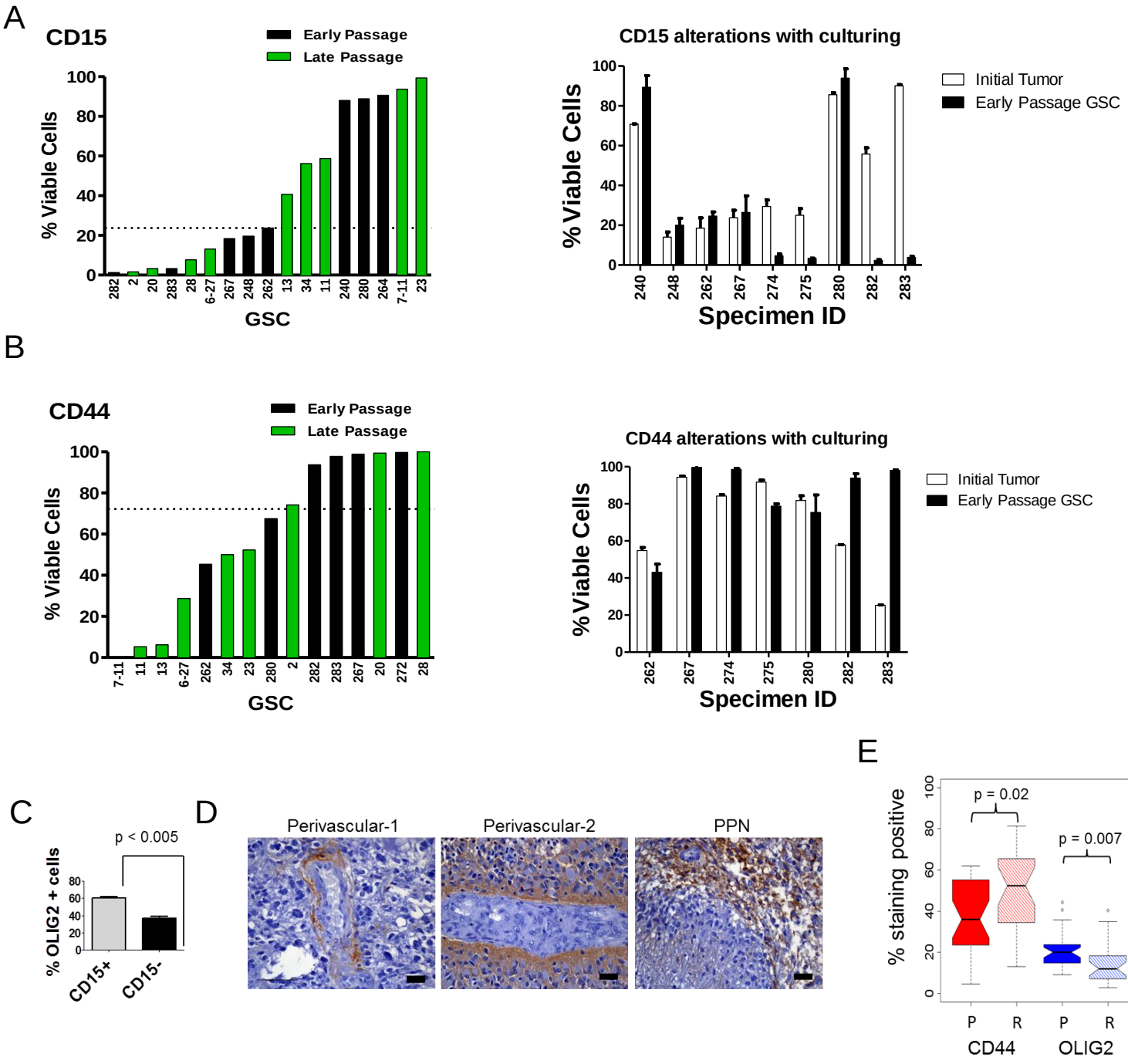
A
CD15
Early Passage
Late Passage
% Viable Cells
GSC
282 2 20 283 28 6-27 267 248 262 13 34 11 240 280 264 7-11 23
CD15 alterations with culturing
Initial Tumor
Early Passage GSC
% Viable Cells
Specimen ID
240 248 262 267 274 275 280 282 283
B
CD44
Early Passage
Late Passage
% Viable Cells
GSC
7-11 11 13 6-27 262 34 23 280 2 282 283 267 20 272 28
CD44 alterations with culturing
Initial Tumor
Early Passage GSC
% Viable Cells
Specimen ID
262 267 274 275 280 282 283
C
p < 0.005
% OLIG2 + cells
CD15+
CD15-
D
Perivascular-1
Perivascular-2
PPN
E
p = 0.02
p = 0.007
% staining positive
P R P R
CD44 OLIG2
F
GSC 34
GSC 11
GSC 262
YKL40 CTGF CD44 FN1
Fold change versus CD15low/CD44low
CD15high/CD44low
CD15low/CD44high
CD15high/CD44high
* p < 0.05

Figure S3, related to Figure 3.

(A) Flow cytometry analysis of percentage of viable CD15 expression in early or late passage GSCs is shown on the left panel. Flow cytometric comparison of CD15 expression in the initial parental GBMs and the isolated early passage GSCs from the same tumor is shown on the right. Error bar indicates +/- SD.

(B) Flow cytometry analysis of percentage of viable CD44 expression in early or late passage GSCs is shown on the left panel. Flow cytometric comparison of CD44 expression in the initial parental GBMs and the isolated early passage GSCs from the same tumor is shown on the right. Error bar indicates +/- SD. Note that while early (<5) versus late (>20) passage of GSCs did not influence the proportion of CD15 or CD44, a subset of the GSCs (282 and 283) lost CD15 expression and gained CD44 in culture when compared to their parental tumors.

(C) Quantification of immunofluorescent analysis of CD15 sorted GSC34 cells plated onto laminin/poly-L-ornithine coated coverslips and stained for OLIG2. Bars represent average percentage expression of OLIG2 in ten random fields against DAPI stained nuclei. Error bar indicates +/- SEM.

(D) IHC staining of CD44 in multiple GBMs. Representative staining shows enrichment of CD44 staining on perivascular niche (left and middle panel) or regions surrounding pseudopalisading necrosis (PPN, right panel). Scale Bar: 20 μm. Note that while CD44 was expressed throughout the tumor in the positive cases, enrichment around the perivascular niche as well as areas surrounding pseudo-palisading necrosis were frequently seen similar to other tumor initiating markers.

(E) Quantification of percentage of CD44 and OLIG2 positive cells in human primary (P) tumors and matched recurrent tumors (R) quantified in ten random fields (n = 30). Bar plots show the range of expression and outliers. p value was determined by Wilcoxon rank-sum test.

(F) Relative mRNA levels of MES genes determined by qRT-PCR of FACS sorted CD15 and CD44 subpopulation in GSCs. Bar graphs represent fold change of the transcript in various quadrants compared to $CD15^{low}/CD44^{low}$ populations. Error bar represents +/- SD. *t* test was used to assess statistical significance.

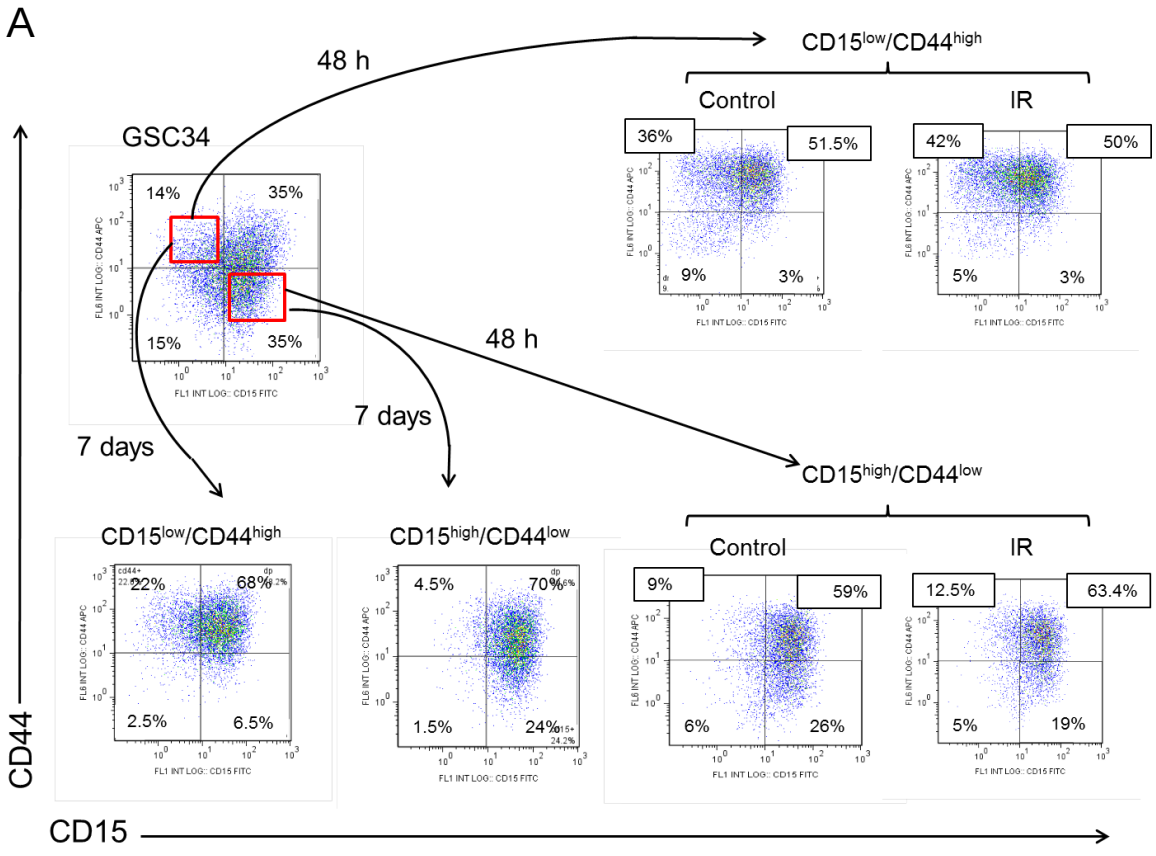
A
GSC34
48 h
7 days
7 days
48 h
CD15low/CD44high
Control
IR
36%
51.5%
9%
3%
42%
50%
5%
3%
14%
35%
15%
35%
CD15high/CD44low
Control
IR
9%
59%
6%
26%
12.5%
63.4%
5%
19%
CD15low/CD44high
22%
68%
2.5%
6.5%
CD15high/CD44low
4.5%
70%
1.5%
24%
CD44
CD15

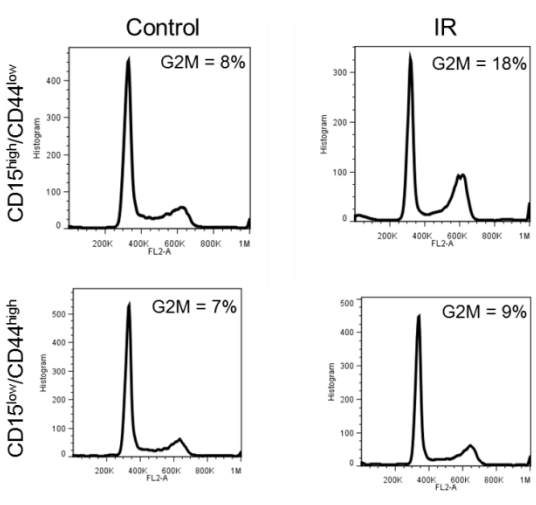
B
Control
IR
CD15high/CD44low
G2M = 8%
G2M = 18%
CD15low/CD44high
G2M = 7%
G2M = 9%
Histogram
FL2-A

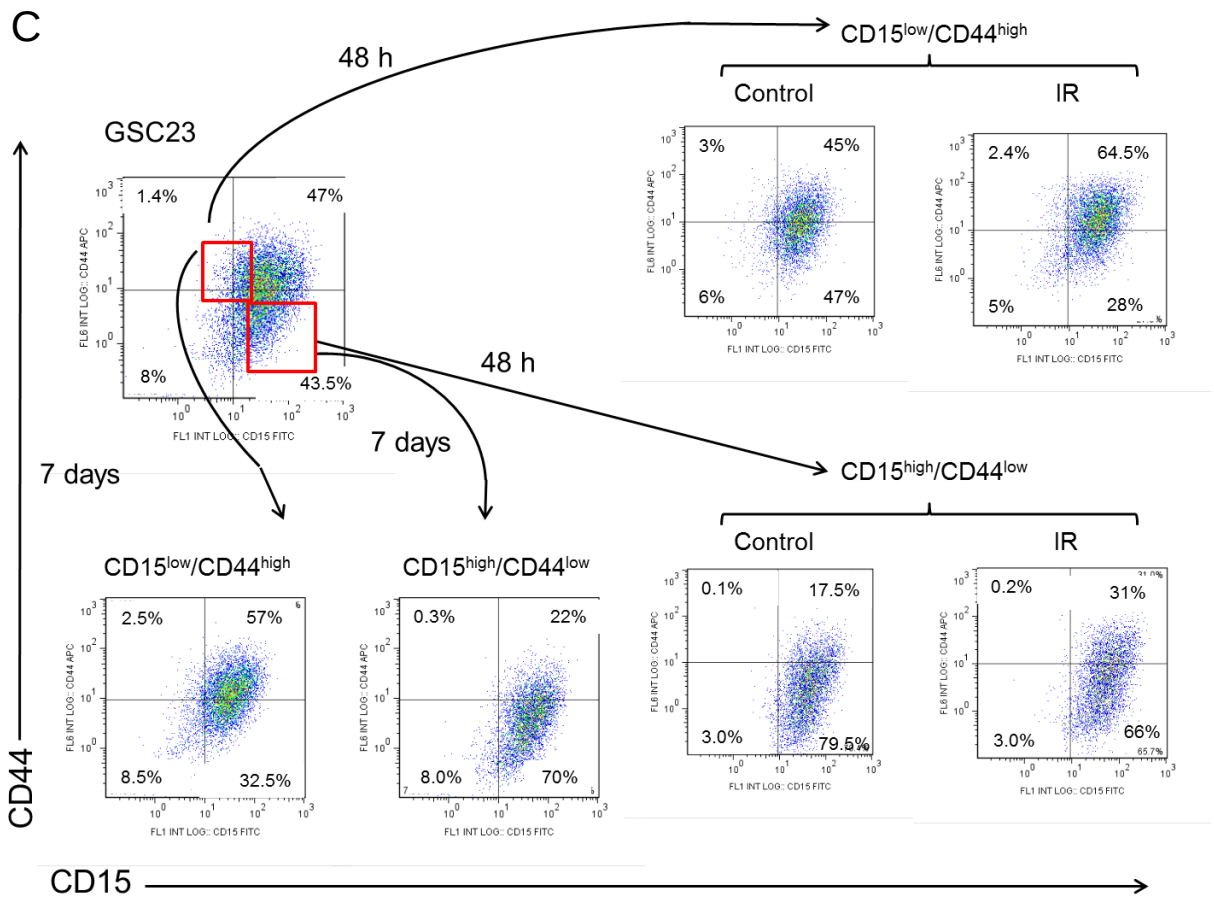

Figure S4, related to Figure 4.

(A) FACS analysis and sorting of CD15^{high} and CD44^{high} in GSC34 (shown in red boxes). Sorted populations were cultured for an additional 7 days to detect changes in the CD15^{high} and CD44^{high} population over time (lower panels). In parallel, 24h after sorting, cells were exposed to 6 Gy IR and analysed for percentage of CD15^{high} and CD44^{high} population for an addional 48 h (right panels). Percentage of cells in each quadrant is shown.

(B) Cell cycle analysis of CD15^{high} and CD44^{high} populations of GSC34 treated with 6 Gy IR. The percentage of cells in the G2/M phase is indicated within each cell cycle plot.

(C) FACS analysis and sorting of CD15^{high} and CD44^{high} in GSC23 (shown in red boxes) as described in S4A. For results shown in Figure 4, PN GSCs that expressed both CD15 and CD44 were sorted into CD15^{high}/CD44^{low} and CD15^{low}/CD44^{high} to see if the enrichment of populations with differential cell surface markers (that correlates with PN/MES states) from within single GSC cultures show differences in response to radiation. GSC34 had sufficient cells from both CD15^{high} and CD44^{high} groups and we tested for alteration in cell surface markers over time and in response to radiation. Despite originating from CD15^{high} or CD44^{high} subpopulation, 48h after sorting, populations became enriched for CD44 and CD15 expression

respectively. The general tendency was to accumulate double positive populations within a short period of time highlighting the inherent plasticity of expression of these cell surface markers. Treatment with radiation caused a mild increase in the CD44 population. At these time points, an increase in G2/M was restricted to the $CD15^{high}$ but not the $CD44^{high}$ subgroup implying the cells in a MES state (as marked by $CD44^{high}$ expression) were indeed radio-resistant. A similar response was seen with GSC23, where the accumulation of $CD44^{high}$ population in response to radiation was profound. Given the plasticity in these states long-term neurosphere assays and orthotopic studies in mice were not feasible.

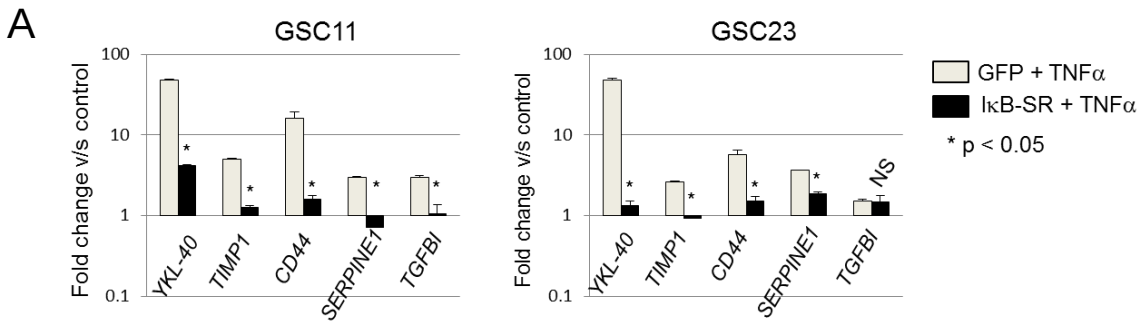
A
GSC11
GSC23
Fold change v/s control
100
10
1
0.1
YKL-40
TIMP1
CD44
SERPINE1
TGFBI
NS
GFP + TNFα
IκB-SR + TNFα
* p < 0.05

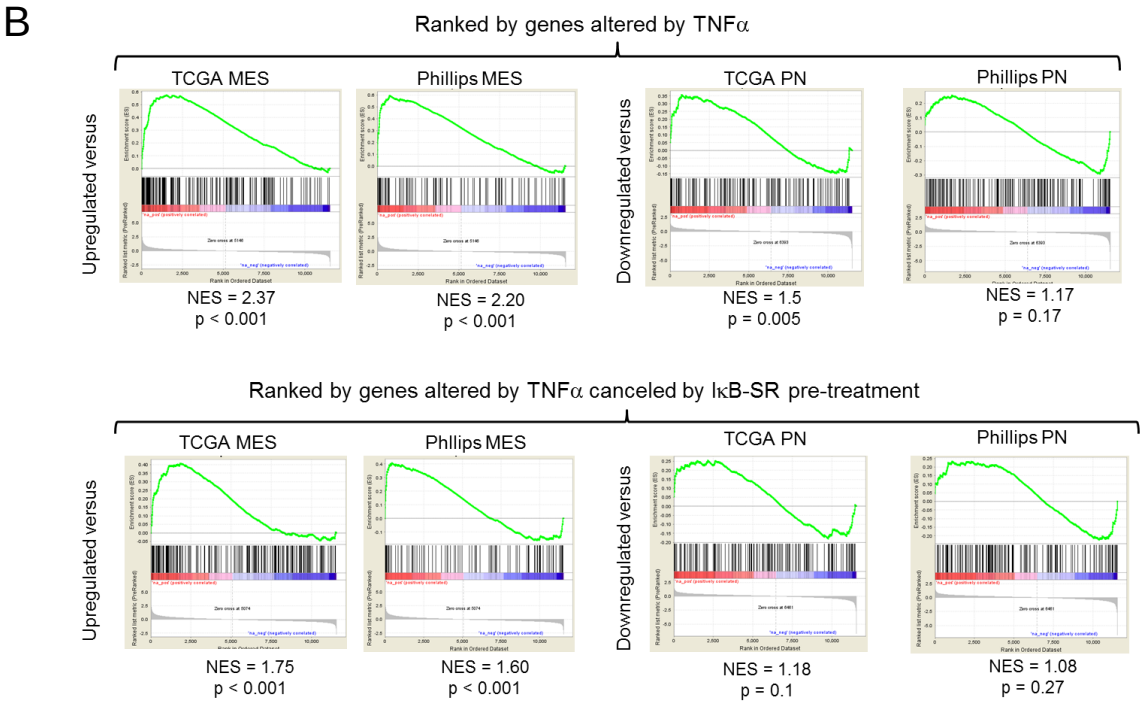
B
Ranked by genes altered by TNFα
TCGA MES
Phillips MES
TCGA PN
Phillips PN
Upregulated versus
Downregulated versus
NES = 2.37
p < 0.001
NES = 2.20
p < 0.001
NES = 1.5
p = 0.005
NES = 1.17
p = 0.17
Ranked by genes altered by TNFα canceled by IκB-SR pre-treatment
TCGA MES
Phllips MES
TCGA PN
Phillips PN
Upregulated versus
Downregulated versus
NES = 1.75
p < 0.001
NES = 1.60
p < 0.001
NES = 1.18
p = 0.1
NES = 1.08
p = 0.27

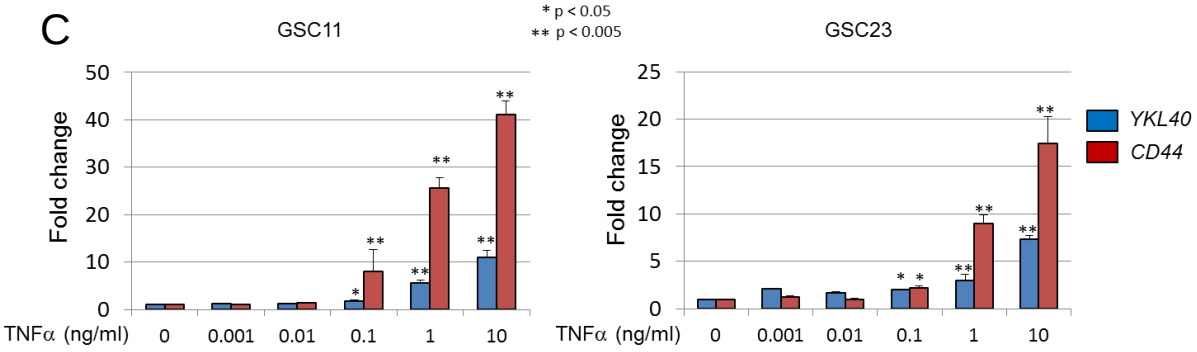
C
* p < 0.05
** p < 0.005
GSC11
GSC23
Fold change
50
40
30
20
10
0
25
20
15
10
5
TNFα (ng/ml)
0
0.001
0.01
0.1
1
10
YKL40
CD44

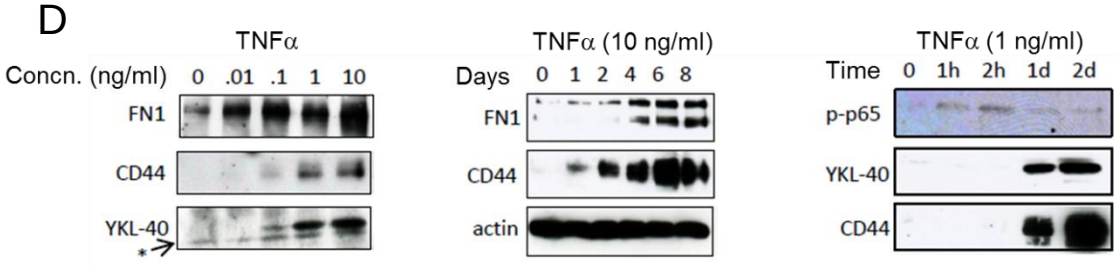
D
TNFα
Concn. (ng/ml) 0 .01 .1 1 10
FN1
CD44
YKL-40
TNFα (10 ng/ml)
Days 0 1 2 4 6 8
FN1
CD44
actin
TNFα (1 ng/ml)
Time 0 1h 2h 1d 2d
p-p65
YKL-40
CD44

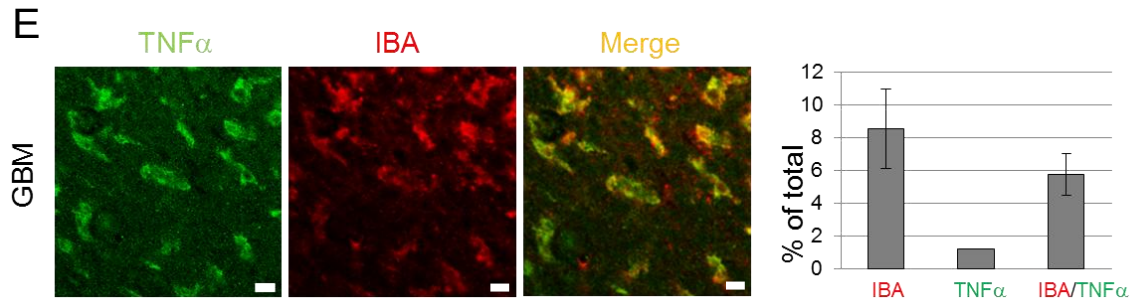
E
TNFα
IBA
Merge
GBM
% of total
IBA
TNFα
IBA/TNFα

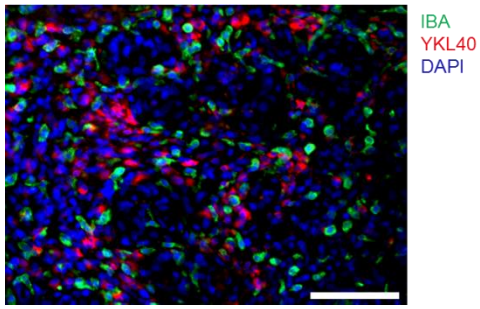
F
IBA
YKL40
DAPI

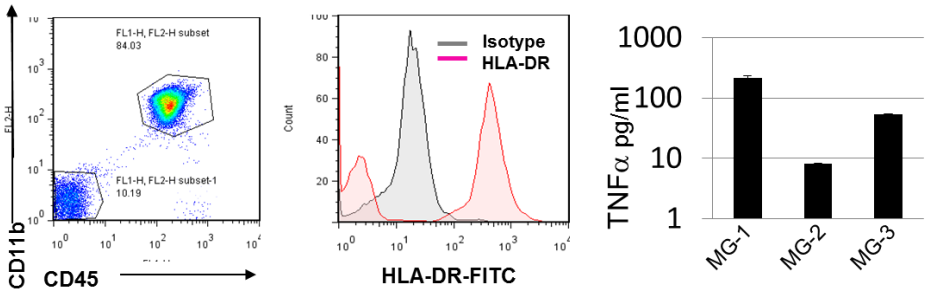
G
CD11b
CD45
Isotype
HLA-DR
HLA-DR-FITC
TNFα pg/ml
MG-1
MG-2
MG-3

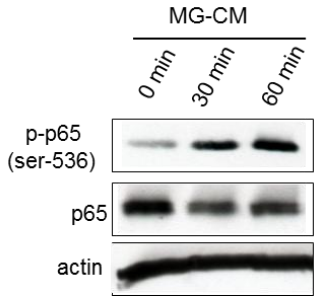
H
MG-CM
0 min
30 min
60 min
p-p65 (ser-536)
p65
actin

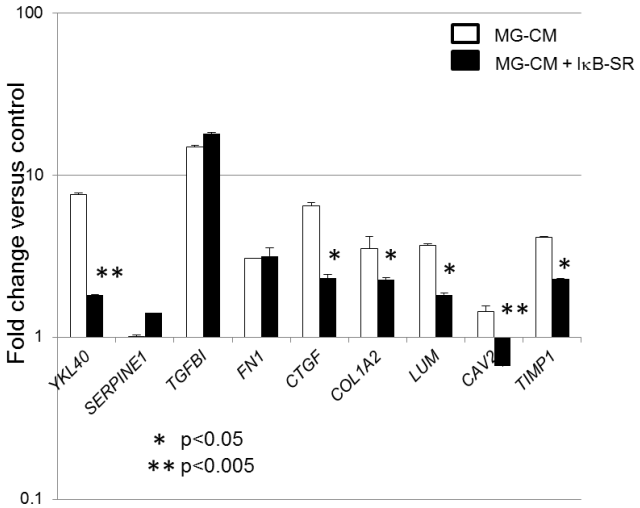
I
MG-CM
MG-CM + IκB-SR
Fold change versus control
YKL40
SERPINE1
TGFBI
FN1
CTGF
COL1A2
LUM
CAV2
TIMP1
* p<0.05
** p<0.005

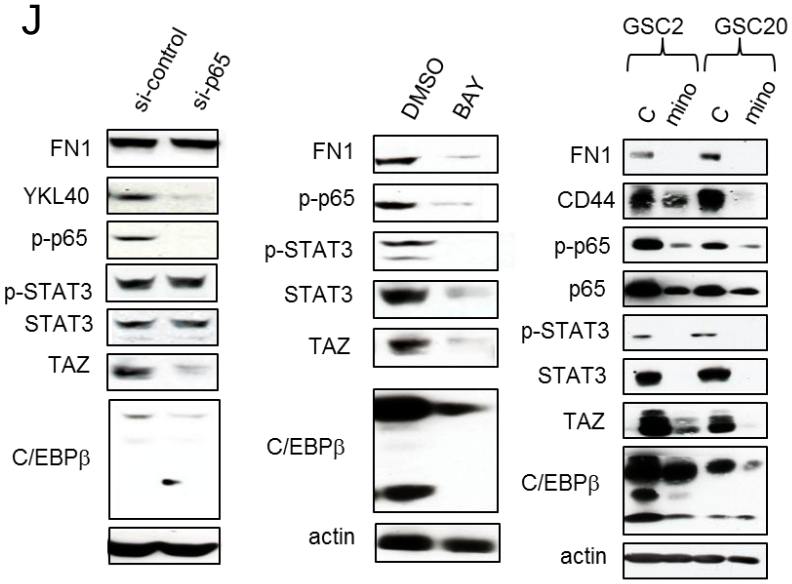
J
si-control
si-p65
FN1
YKL40
p-p65
p-STAT3
STAT3
TAZ
C/EBPβ
DMSO
BAY
FN1
p-p65
p-STAT3
STAT3
TAZ
C/EBPβ
actin
GSC2
GSC20
C
mino
C
mino
FN1
CD44
p-p65
p65
p-STAT3
STAT3
TAZ
C/EBPβ
actin

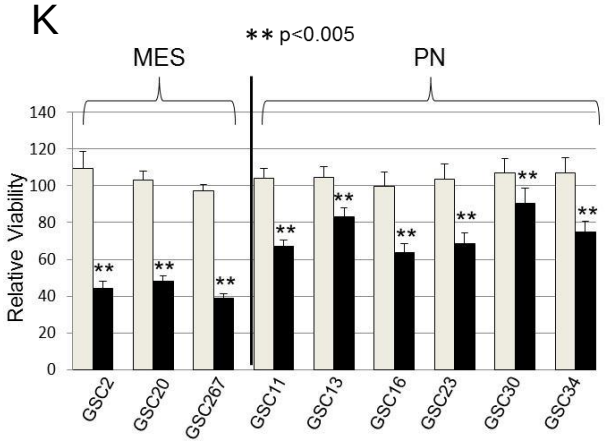
K
** p<0.005
MES
PN
Relative Viability
GSC2
GSC20
GSC267
GSC11
GSC13
GSC16
GSC23
GSC30
GSC34

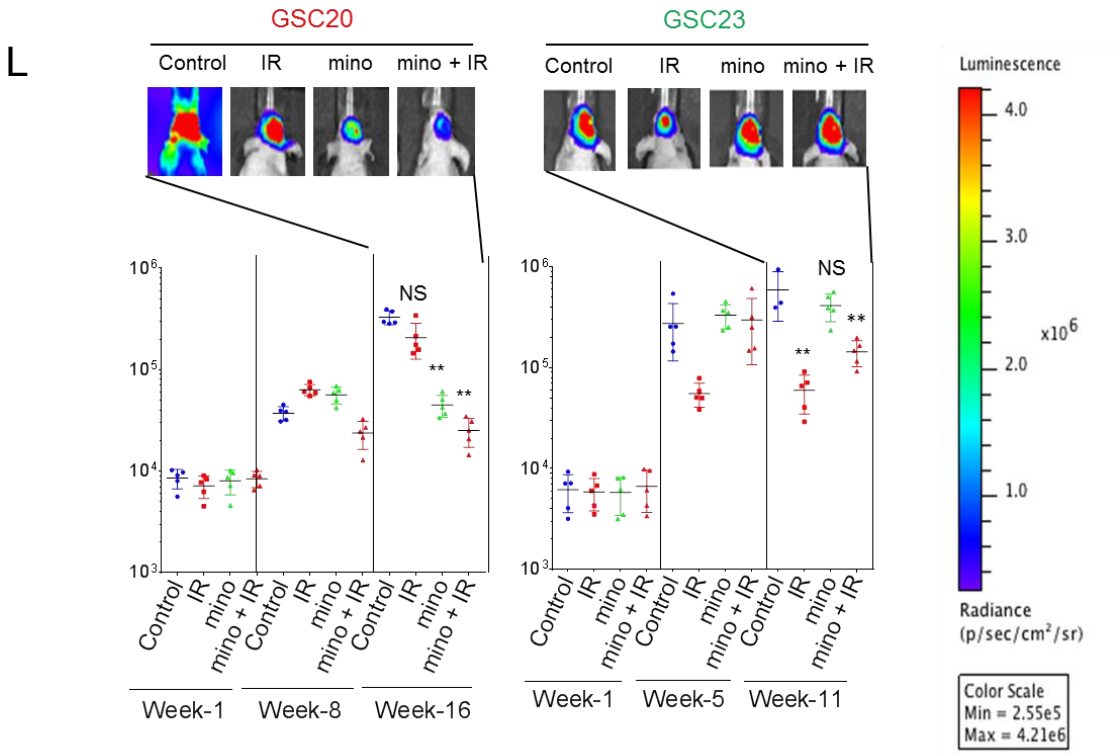
L
GSC20
GSC23
Control
IR
mino
mino + IR
Luminescence
4.0
3.0
2.0
1.0
x10^6
Radiance (p/sec/cm²/sr)
Color Scale
Min = 2.55e5
Max = 4.21e6
NS
**
Week-1
Week-8
Week-16
Week-5
Week-11

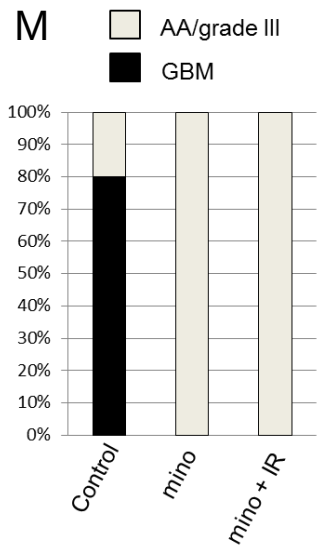
M
AA/grade III
GBM
100%
90%
80%
70%
60%
50%
40%
30%
20%
10%
0%
Control
mino
mino + IR

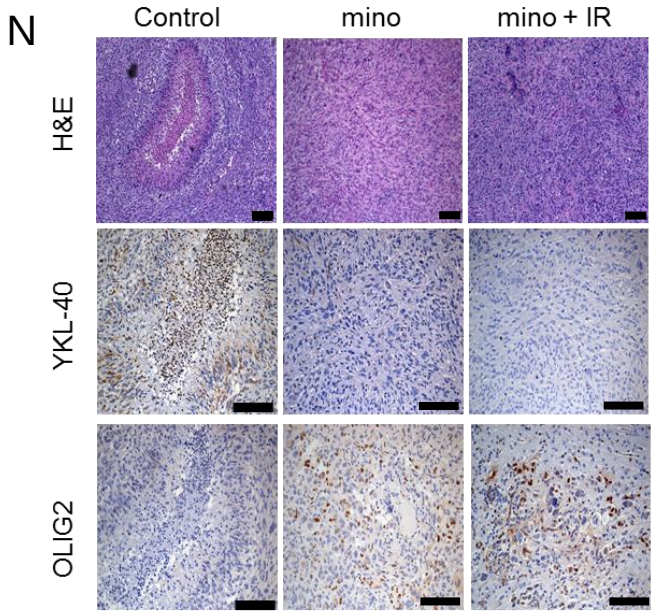
N
Control
mino
mino + IR
H&E
YKL-40
OLIG2

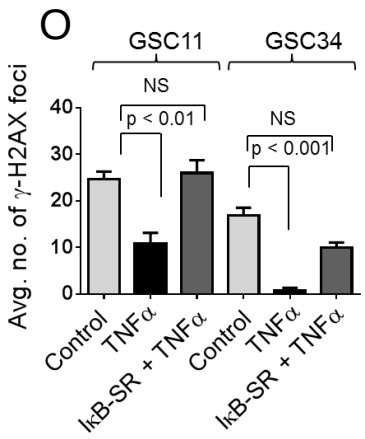
O
GSC11
GSC34
NS
p < 0.01
NS
p < 0.001
Avg. no. of γ-H2AX foci
Control
TNFα
IκB-SR + TNFα

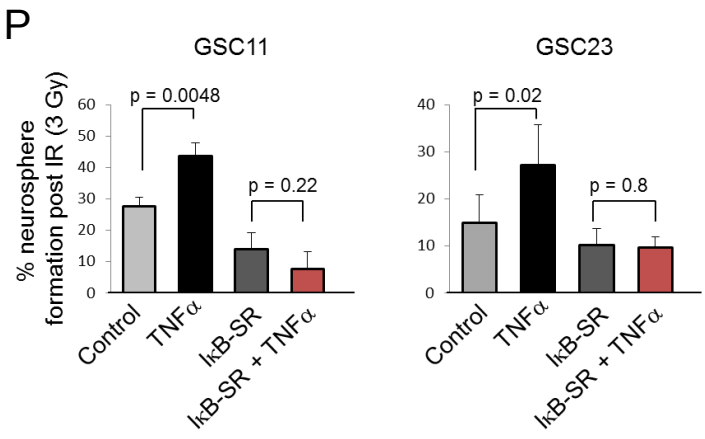
P
GSC11
GSC23
p = 0.0048
p = 0.22
p = 0.02
p = 0.8
% neurosphere formation post IR (3 Gy)
Control
TNFα
IκB-SR
IκB-SR + TNFα

Figure S5, related to Figure 5.

(A) qRT-PCR analysis of MES genes in GSC11 and GSC23 after treatment with TNFα (48 h, 10 ng/ml) with or without pre-treatment with IκB-SR or control GFP adenovirus 24 h prior to TNFα treatment. Bar graphs indicate average of triplicate measurements and plotted as fold change of TNFα treated versus untreated groups. Error bar indicates +/- SD. Statistical significance was assessed using *t* test.

(B) GSEA analysis of TNFα altered genes (1.5 fold or greater) (top) or TNFα-altered genes suppressed by IκB-SR pre-treatment (bottom). Comparison was made against Phillips or TCGA GBM MES and PN signatures.

(C) Upper panel shows the qRT-PCR analysis of dose response induction of *CD44* and *YKL40* in GSC11 (left) GSC23 (right) after 24h treatment with varying concentrations of TNFα. Bar graph shows relative expression of *CD44* and *YKL40* to cells without TNFα treatment. Error bar indicates +/- SD. *t* test was used to assess statistical significance.

(D) Western analysis of induction of FN1, CD44, YKL40 and p-p65 after TNFα treatment in GSC11. Left panel is the dose response induction of MES markers and the start indicates a non-specific band. The middle panel shows the time course and the right panel shows that induction of p-p65 precedes expression of YKL-40 upon treatment of TNFα.

(E) To examine potential sources of TNFα that could serve to maintain the MES phenotype in human GBM tumors we performed immunofluorescent staining with IBA (red), a marker that identifies macrophages/microglia, and we observed significant co-localization of IBA with TNFα. Bar graph shows percentage cells positive for each marker in three independent fields. Error bar indicates +/- SEM. Scale bar: 20 μm.

(F) Immunofluorescent staining for YKL-40 and IBA in GBMs. YKL40 expression is shown in red and IBA is shown in green. Merged image of both proteins is shown against DAPI positive nuclei (blue). Scale bar: 100μm. Note that the two proteins rarely showed co-localization.

(G) Rapid isolation protocol for enrichment of macrophages/microglia using differential Percoll gradient from human surgical glioma samples. Left panel shows the FACS analysis of expression of CD11b and CD45 in isolated macrophages/microglia that were of high purity. Middle panel shows that isolated macrophages/microglia are HLA-DR^{+} suggesting activation phenotype. ELISA analysis of secreted TNFα in the media of three independent acutely isolated macrophages/microglia. Bar graph shows average levels of TNFα secreted in the conditioned media after 48-96 h in culture. Error bar indicates +/- SEM.

(H) Western analysis shows the induction of p-p65 in GSC11 after addition of pooled rapidly isolated macrophages/microglia conditioned media (MG-CM) at the indicated timepoints.

(I) qRT-PCR analysis of MES genes in GSC11 after treatment with pooled macrophages/microglia conditioned media (MG-CM, n = 3) with or without pre-treatment with IκB-SR or control GFP adenovirus 24 h prior to exposure to MG-CM treatment. Treating GSC11 with MG-CM caused induction of MES genes, and this effect was significantly reduced

by pre-treatment with IκB-SR indicating that NF-κB activation by factors derived from macrophages/microglia can lead to MES differentiation of PN GSCs. We could not ascertain the specific contribution of TNFα in the MG-CM to MES differentiation since these samples were limited. Bar graphs indicate average of triplicate measurements and plotted as fold change of MG-CM treated versus untreated groups. Statistical significance was assessed using *t* test. Error bar indicates +/- SEM.

(J) Western blot analysis of MES markers and master TFs STAT3, C/EBPβ and TAZ after treating indicated MES GSCs with si-p65 for 72 h (left panel), BAY 11-7082 (10 μM) for 96 h (middle panel) and minocycline (50 μM) for 5 days (right panel). We raised the possibility that silencing NF-κB may impact the MES state of these cells. Consistently, transient knockdown of p65 was sufficient to reduce protein levels of YKL40, TAZ, and C/EBPβ, but not STAT3, implying that the p65 subunit is not required for maintenance of STAT3 expression. However, treatment of cells with IκB kinase inhibitor, BAY 11-7082, caused a decrease in expression of all three TFs suggesting that while the p65 subunit of NF-κB alone was not sufficient to alter STAT3, global inhibition of the NF-κB pathway had a suppressive effect on STAT3 expression. *In vitro* treatment of GSC2 and GSC20 also caused dramatic reduction of master TF expression as well as CD44 and FN1 within 4 days.

(K) Cell viability was detected using the WST-1 assay. Bar graphs indicate percentage of cells viable after a 5 day minocycline treatment (black bars) against untreated controls (gray bars). Error bar indicates +/- SD. *t* test was used for statistical significance. We observed a more profound minocycline induced reduction of cell viability of MES GSCs in comparison to PN GSCs.

(L) Representative bio-luminescence images of GSC20 (left panel) or GSC23 (right panel) transduced with pCignal lenti-CMV-luc injected into Foxn1^{nu} mice. Cells were imaged 2-3 weeks after implantation as the first timepoint (week 1) after which the radiation group received four cycles of 2.5 Gy IR on consecutive days. We treated mice bearing xenografts with 50 mg/kg minocycline starting four days prior to radiation. Minocycline treatment strongly reduced tumor growth in X-GSC20 and the effect was additive when combined with radiation, while radiation alone had modest, but not statistically significant reduction in tumor volume compared to the control group. To test whether the effect of minocycline was specific for the MES GSCs, we treated implanted GSC23 intracranially into mice and followed the same treatment regimen as GSC20. As expected, radiation caused a decrease in tumor volume compared to control groups but minocycline had no significant effect on tumor size (right panel). Thus, minocycline specifically had antitumor effects only on MES GSCs in the xenograft model. Black bar shows average radiance (photons/s/cm^2/sr) with various treatments and time points. Error bar indicates +/- SEM. Color key for luminescence is shown on the right. *t* test was used to assess statistical significance. NS = not significant.

(M) Stacked bar graph shows percentage of mice exhibiting features of AA or GBM within each group. To discern if minocycline treatment influenced tumor grade, we inspected hematoxylin and eosin (H&E) stained sections from all groups. Tumors from GSC20 injected mice predominantly showed features of GBM (with tumor necrosis), whereas those treated with minocycline lacked necrosis while still exhibiting features of grade III AAs.

(N) IHC analysis of various markers in GSC20 xenograft tumors that were treated with minocycline alone or in combination with IR compared to untreated mice. Upper panel shows the representative H&E staining. Middle and lower panel show the expression of YKL-40 and OLIG2 respectively. A significant reduction in the expression of YKL40 and CD44 (data not shown) was seen in all tumors treated with minocycline. A subset of mice treated with minocycline (n = 2 out of 5) and those with both minocycline and radiation (n = 2 out of 5) showed OLIG2 staining in about 10-60% of the tumor area, although the induction of PN genes was not seen *in vitro*. Scale bar: 100 μm.

(O) GSCs were treated with TNFα for 96 h with or without pre-treatment with IκB-SR or control GFP adenovirus 24 h prior to TNFα treatment followed by plating onto glass slides coated with laminin/poly-L-ornithine. 24 h later, cells were irradiated with 3 Gy and immunostained with anti-γ-H2AX antibody and the number of foci per nuclei was counted. Bar graphs indicate average number of foci per nuclei in at least 25 nuclei. Error bar indicates +/- SD. Statistical significance was assessed using *t* test.

(P) Bar graphs indicate the average percentage of neurosphere formation of post irradiated GSCs compared to control group. Error bar indicates +/- SD. Statistical significance was assessed using *t* test.

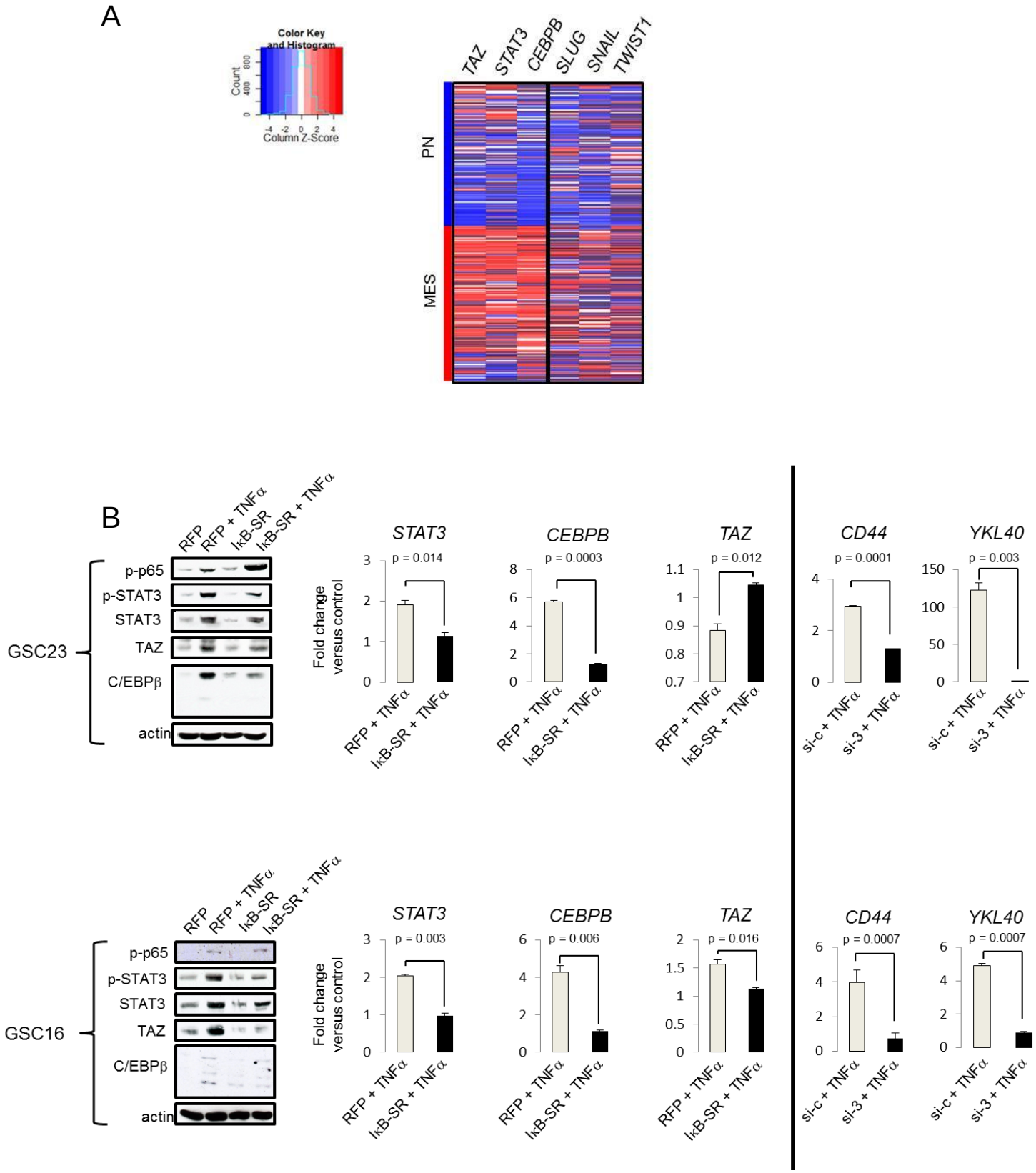
A
Color Key and Histogram
Count
Column Z-Score
TAZ
STAT3
CEBPB
SLUG
SNAIL
TWIST1
PN
MES
B
RFP
RFP + TNFα
IκB-SR
IκB-SR + TNFα
GSC23
p-p65
p-STAT3
STAT3
TAZ
C/EBPβ
actin
Fold change versus control
STAT3
p = 0.014
CEBPB
p = 0.0003
TAZ
p = 0.012
CD44
p = 0.0001
YKL40
p = 0.003
RFP + TNFα
IκB-SR + TNFα
si-c + TNFα
si-3 + TNFα
GSC16
STAT3
p = 0.003
CEBPB
p = 0.006
TAZ
p = 0.016
CD44
p = 0.0007
YKL40
p = 0.0007

Figure S6, related to Figure 6.

(A) Heatmap showing the expression of master TFs, *STAT3, CEBPB, TAZ*, and EMT inducers, *SNAIL, SLUG* and *TWIST1* in PN and MES tumors from the TCGA.

(B) Left panel shows the western blot analysis of MES master TFs markers STAT3, C/EBPβ and TAZ in GSC23 and GSC16 pre-treated with IκB-SR or control RFP for 36 h prior to TNFα treatment for an additional 24h. Bar graphs show the qRT-PCR analysis of master TFs after similar treatments as above. Right panel shows qRT-PCR analysis of *YKL40*, and *CD44* gene expression after knockdown of all three master TFs (STAT3, C/EBPβ and TAZ). Cells were treated with siRNA 72h prior to treatment with TNFα for an additional 24 h. *t* test was used for statistical significance.

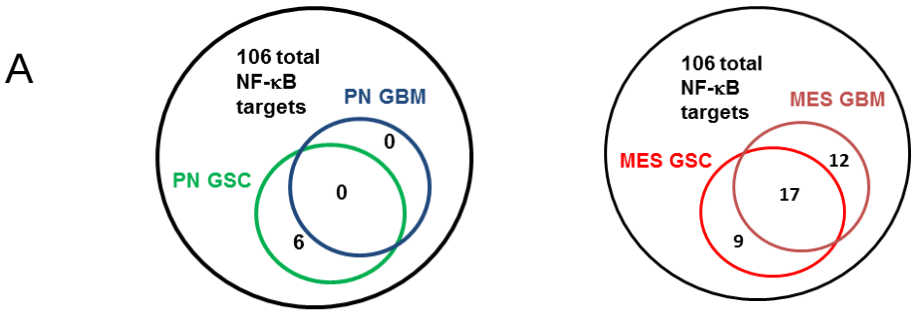


```
$Venn_List$NF.kBGSC
[1] "CCND1" "CD74"  "MYC"   "PTX3"  "TNC"   "TP53"
```

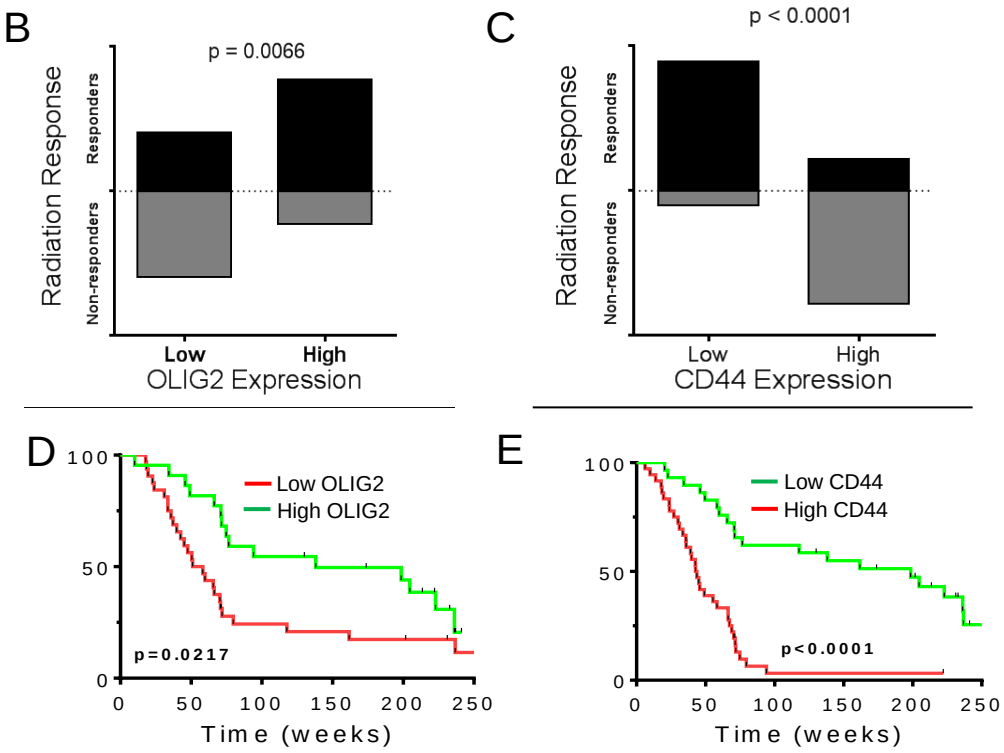

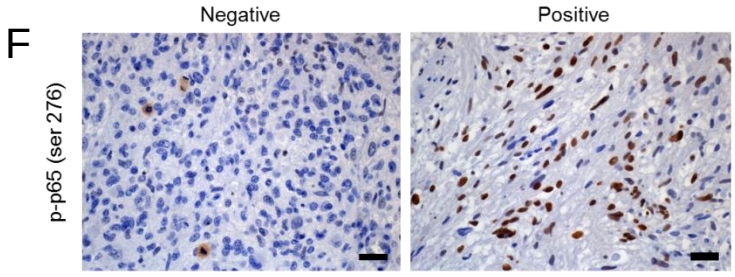

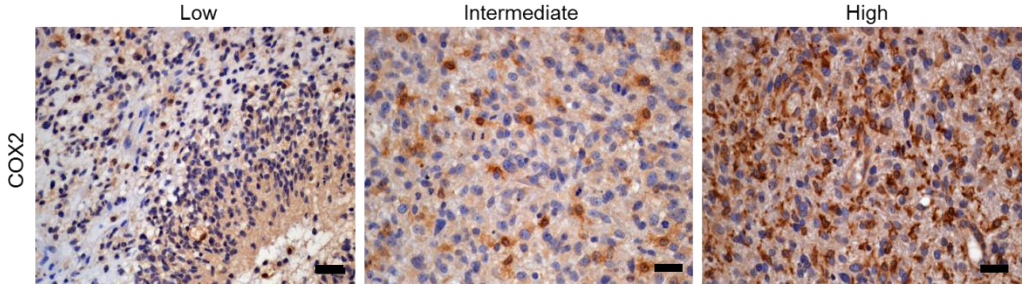

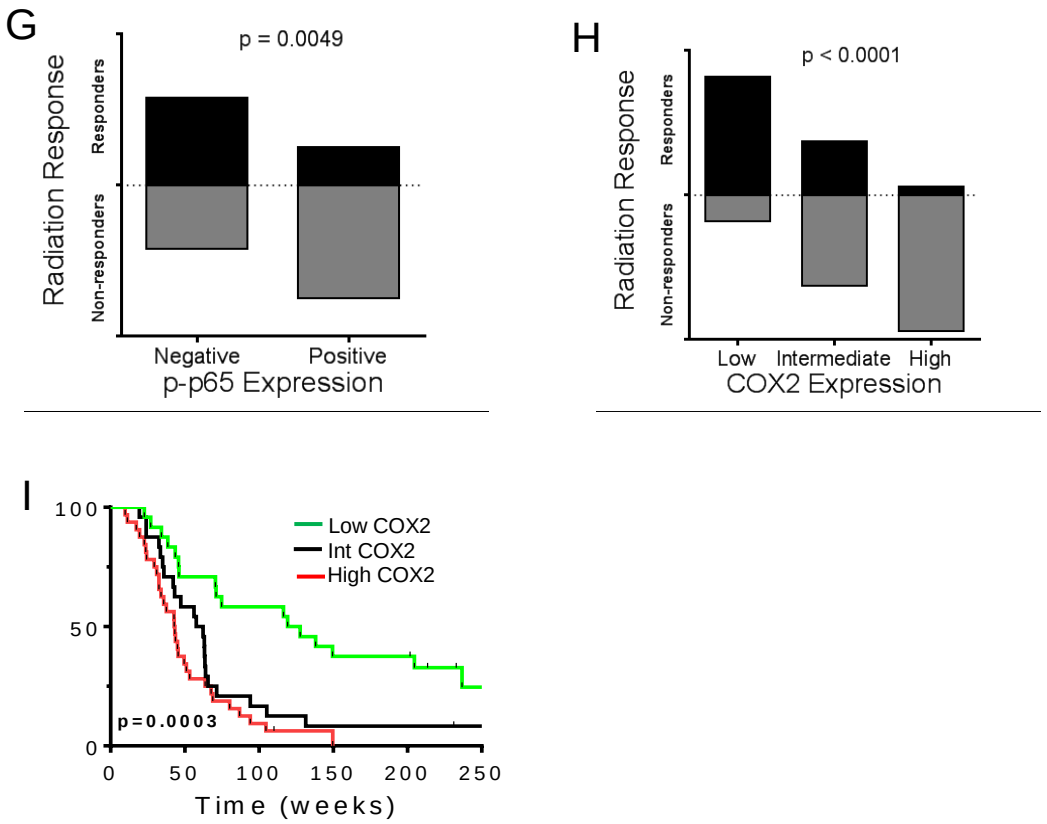

Figure S7, related to Figure 7.

(A) Venn diagram showing overlap of NF-κB target genes between PN/MES GBMs from TCGA and PN/MES GSCs from our study that showed 1.5 fold or greater induction compared to tumors/GSCs. The NF-κB targets enriched in the PN tumors/GSCs (v/s MES) are shown below, whereas those enriched in MES tumors/GSCs (v/s PN) are listed in Table S6.

(B) Bar graph showing the proportion of OLIG2, and (C) CD44 expression in newly diagnosed GBM patients classified as RT responders or non-responders. Chi square test was used to assess statistical significance. Number of samples tested for each marker is shown in Table S7. Kaplan Meier curves showing survival of newly diagnosed GBM patients based on OLIG2 (D), and CD44 (E) is shown below. Log rank test was used to assess statistical significance.

(F) Representative IHC staining of GBM tissues with p-p65 (ser 276, above) and COX2 (below) is shown. Scale bar: 20μm.

(G) Bar graph showing the proportion of p-p65, or (H) COX2 expression in newly diagnosed GBM patients classified as RT responders or non-responders. Chi square test was used to assess statistical significance. Number of samples tested for each marker is shown in Table S7.

(I) Kaplan Meier curves showing survival of newly diagnosed GBM patients based on COX2 is shown Log rank test was used to assess statistical significance.

Table S6 related to Figure 7. NF-κB target genes specific to the MES subtype

Gene Symbol	Description	GSC	GBM
CD44	CD44 molecule (Indian blood group)	+	+
CCL2	chemokine (C-C motif) ligand 2	+	+
CXCL5	chemokine (C-X-C motif) ligand 5	+	+
HMOX1	heme oxygenase (decycling) 1	+	+
IER3	immediate early response 3	+	+
ICAM1	intercellular adhesion molecule 1	+	+
IRF1	interferon regulatory factor 1	+	+
IL1B	interleukin 1, beta	+	+
IL15	interleukin 15	+	+
IL15RA	interleukin 15 receptor, alpha	+	+
IL8	interleukin 8	+	+
NQO1	NAD(P)H dehydrogenase, quinone 1	+	+
PTGS2	prostaglandin-endoperoxide synthase 2 (prostaglandin G/H synthase and cyclooxygenas	+	+
PSMB9	proteasome (prosome, macropain) subunit, beta type, 9 (large multifunctional peptidase 2	+	+
S100A6	S100 calcium binding protein A6	+	+
TFPI2	tissue factor pathway inhibitor 2	+	+
TNFAIP3	tumor necrosis factor, alpha-induced protein 3	+	+
BCL2A1	BCL2-related protein A1	-	+
CD48	CD48 molecule	-	+
CCL5	chemokine (C-C motif) ligand 5	-	+
CCR5	chemokine (C-C motif) receptor 5	-	+
FAS	Fas (TNF receptor superfamily, member 6)	-	+
IL6	interleukin 6 (interferon, beta 2)	-	+
MMP9	matrix metallopeptidase 9 (gelatinase B, 92kDa gelatinase, 92kDa type IV collagenase)	-	+
PTX3	pentraxin 3, long	-	+
PLAU	plasminogen activator, urokinase	-	+
SOD2	superoxide dismutase 2, mitochondrial	-	+
TNC	tenascin C	-	+
VCAM1	vascular cell adhesion molecule 1	-	+
CSF2	colony stimulating factor 2 (granulocyte-macrophage)	+	-
IRF2	interferon regulatory factor 2	+	-
IRF7	interferon regulatory factor 7	+	-
IL1A	interleukin 1, alpha	+	-
IL11	interleukin 11	+	-
NFKBIA	nuclear factor of kappa light polypeptide gene enhancer in B-cells inhibitor, alpha	+	-
NOD2	nucleotide-binding oligomerization domain containing 2	+	-
STAT5A	signal transducer and activator of transcription 5A	+	-
VEGFC	vascular endothelial growth factor C	+	-

List of published NF-κB target genes that show 1.5 or greater expression in the MES class compared to PN is shown. Genes that are relatively higher in either or both TCGA tumors as well as GSCs are shown with a “+”.

Table S7 related to Figure 7. Cohort of patients used for clinical analyses

Parameter	Number (percentage)
Total no. of patients	206 (100)
Age (median, range) in years	56.9 (18.9-84.2)
Follow-up (median, range) in weeks	64.7 (6.1-673)
	Censored=28 (14)
Vital status	Deceased=176 (85)
	Unknown=2 (1)
	50=1 (0.5)
	60=7 (3)
Karnofsky Performance Status	70=15 (7)
	80=45 (22)
	90=87 (42)
	100=18 (9)
	Unknown=33 (16)
	Stable/Responders=105 (51)
RT Response	Non-responders=99 (48)
	Unknown=2 (1)
	Mutant=122 (59)
***IDH1* Status**	Wild-type=21 (10)
	Unknown=63 (31)
	High=37 (18)
CD44	Low=29 (14)
	Unknown=140 (68)
	High=23 (11)
OLIG2	Low=32 (16)
	Unknown=151 (74)
	High=53 (26)
p-p65	Low=27 (13)
	Unknown=126 (61)
	High=33 (16)
COX2	Intermediate=24 (12)
	Low=24 (12)
	Unknown=125 (60)

Table S8 related to Figure 7. Data showing significant predictors of radiation response using a generalized linear model.

Variable	Parameter Estimate	95% CI	p value
MES (low vs. high)	-0.73	-1.22 to -0.28	0.0014
IDH1 (WT vs. mutant)	-0.09	-0.75 to 0.56	0.7738
KPS (≤70 vs >70)	-0.78	-1.99 to 0.32	0.1661
Age (≤50 vs >50	0.27	-0.66 to 1.20	0.569

Table S9 related to Figure 8. Serial section IHC of various markers in newly diagnosed GBM

	OLIG2	CD44	p-p65	IBA
GBM1				
1	INT	LOW	+	INT
2	LOW	HIGH	+	HIGH
3	INT	HIGH	+	HIGH
GBM2				
1	HIGH	LOW	-	INT
2	HIGH	LOW	-	HIGH
GBM3				
1	HIGH	LOW	-	LOW
2	HIGH	LOW	-	LOW
3	LOW	HIGH	-	HIGH
GBM4				
1	HIGH	LOW	+	INT
2	LOW	HIGH	+	HIGH
3	LOW	HIGH	+	HIGH
GBM5				
1	HIGH	LOW	+	HIGH
2	HIGH	LOW	+	HIGH
GBM6				
1	HIGH	LOW	-	HIGH
2	LOW	HIGH	+	HIGH
3	LOW	HIGH	+	HIGH
GBM7				
1	HIGH	LOW	-	LOW
2	LOW	HIGH	+	HIGH
GBM8				
1	LOW	HIGH	+	HIGH
2	LOW	HIGH	+	HIGH
3	LOW	HIGH	+	HIGH
GBM9				
1	LOW	HIGH	+	HIGH
2	HIGH	LOW	+	INT
3	LOW	HIGH	+	HIGH
GBM10				
1	HIGH	LOW	-	INT
2	HIGH	LOW	-	INT

The expression of OLIG2, CD44, p-p65 (ser 276), and IBA in GBM was analyzed by IHC on consecutive 5 μm sections. Numbers indicate independent areas within each tumor. IBA-specific staining of macrophages/microglia infiltration was classified as low (<10% tumor area), intermediate (10-30%) or high (>30%).

Supplemental Experimental Procedures

Bio-informatic analyses

The top 500 genes with the highest median absolute deviation were identified, then subjected to unsupervised hierarchical cluster analysis, using Cluster 3.0 and Java Treeview (Eisen et al., 1998). Cluster genes were analyzed using the DAVID webtool (http://david.abcc.ncifcrf.gov/) to assign GO categories and plotted as previously described (Dennis et al., 2003). For GSEA analysis, a ranked list of all of the genes on the Affymetrix HGU133A version 2.0 genechips was generated taking the average expression of cluster 2 GSCs minus cluster 1 GSCs for each gene. Independently, ranked gene lists were obtained from previous studies for the MES and PN signatures (Phillips et al., 2006; Verhaak et al., 2010) taking the average expression of the two signatures, generated from the two datasets and subject to GSEA . For the PN/MES metagene calculation (Figures 2A, S2C, and S2G), RNA from GSCs, their respective originating GBM tumor, and mouse xenograft were prepared and the expression of four PN (*DLL3, OLIG2, ASCL1,* and *NCAM1*), and four MES (*YKL40, SERPINE1, TIMP1,* and *TGFBI*) genes were analyzed by qRT-PCR. Using the delta Ct values, composite metagenes were then calculated as noted above, then Z-score corrected, and the PN metagene score was subtracted from the MES score to generate values for a comparative heatmap. A five gene metagene (using *DLL3, OLIG2, YKL40, TGFBI,* and *TIMP1*) was used for Figure 7B and C. For the methylation analysis, DNA isolated from GSCs were profiled using the Illumina Infinium methylation array. For the TCGA samples ($G.CIMP^+$: TCGA-16-0849, TCGA-16-1460; $G\text{-}CIMP^-$: TCGA 02-0052, TCGA 02-0054), level 3 Illumina Infinium data was downloaded. The two sets of data (GSC and TCGA GBM) were batch corrected using the COMBAT algorithm. Methylation probes for the $G\text{-}CIMP^+$ (as identified by Noushmehr et al. 2010) were limited to only those probes available on both methylation platforms were used. All methylation probes in common between the two methylation platforms that had a β-value > 0.5 were used, after filtering out probes that were non-variably methylated among all 9 samples (i.e. hypermethylated to a similar degree in all 9 samples). The G-CIMP methylation signature included PN/hypermethylated genes with a p value cutoff of less than 0.05 (n=1520 transcripts). These genes were then mapped back to Infinium methylation probes (n= 2562 probes). The probe list was further filtered to remove probes that had missing data in the four samples (n = 2480 probes remaining). The complete NF-κB target gene list was downloaded from http://www.bu.edu/nf-kb/gene-resources/target-genes/. Expression of *STAT3, CEBPB,* and *TAZ* was analyzed in three independent published datasets for GBM expression profiles: the Rembrandt (Madhavan et al., 2009) , TCGA (TCGA, 2008) and the Erasmus datasets (Gravendeel et al., 2009). For the NF-κB metagene, the average expression of its downstream targets listed in Table S6 was used. Normalized values were compared across datasets after dividing tumors based on *CD44* expression above or below the median.

LOH analysis

Genomic DNA was isolated from GSCs (Epicenter) following proteinase K treatment. Six microsatellite markers along chromosome 10q were selected for loss of heterozygosity (LOH) analysis. The list of markers and the primers used for PCR are listed in Supplemental Experimental Procedures. The microsatellite marker sequences, size and their corresponding locations on chromosome 10q were obtained from the Cooperative Human Linkage Centre, Genethon and UniSTS. The microsatellite loci were PCR amplified using 50 ng genomic DNA, locus specific FAM-labeled primers and the Amplitaq gold PCR master mix (Applied Biosystems). The PCR products were analyzed with an automated ABI 377 sequencer and Genescan 2.1 software (Applied Biosystems). A heterozygosity index (number of informative cases/total number of cases analyzed per marker) was calculated for each of the six microsatellite markers using normal brain tissue from ten autopsy cases. All of the six markers used in the study had a heterozygosity index of ≥ 0.8. Due to lack of availability of matched normal tissue, an LOH scoring system was devised based on the assumption that if 5 or more of the highly informative markers used in the study were homozygous, a call of LOH would be made.

EGFR amplification

Genomic DNA was subject to real time PCR based copy number assay for EGFR (Hs04942325_cn) and the copy number reference assay HTERT (4403316) from Applied Biosystems. Normal brain DNA was used as the normalizer for copy number calculations. The delta delta Ct method was used with normal brain as the reference to calculate a fold change. Copy number was calculated using the formula 2 x delta delta Ct. Copy number values for the GSC lines were calculated relative to normal brain.

NF1 mutation

PCR products were amplified from genomic DNA templates using primers spanning *NF1* (Parsons et al., 2008) with Platinum Taq polymerase per the manufacturer's protocol. The products were then Sanger sequenced to determine mutations (Beckman Coulter Genomics).

Methylation assay

MethyLight assay was performed as described earlier (Noushmehr et al., 2010) on a panel of eleven markers that included *ANKRD43, HFE, MAL, LGALS3, RHOF, ADPRH, COL21A1, HSD11B2, RAB27B, RILP,* and *SLITL2. COL2A1* was used as a control. Briefly, genomic DNA from all the GSCs and matched human GBM tumors was isolated and bisulfite converted (Zymo Research, Orange, CA), amplified, and detected by MethyLight real-time PCR strategy as described previously (Eads et al., 2000; Eads et al., 1999).

IDH1 mutation analysis

Genomic DNA samples from GSCs were tested for *IDH1* WT and R132H mutation using the Competitive Allele-Specific Taqman PCR (Applied Biosystems). For the tumor specimens, either the PCR method or IHC using an R132H antibody as described below was used.

IHC analysis

Tumors embedded in paraffin blocks were deparaffinized, and hydrated through an ethanol series. After microwave antigen retrieval, antibodies against YKL40 (Santa Cruz), OLIG2 (IBL), Nestin (Santa Cruz), CD44 (BD Biosciences), EGFR (Invitrogen), p-p65 (ser 276, Cell signaling), COX2 (Novus Biologicals), IBA (Waco), or IDH1 mut (specific for R132H, Dianova GmbH) were incubated with the slides overnight at 4°C. Staining was performed using the DAKO Envision kit according to the manufacturer's instructions (DAKO). For frozen sections, fixation of the tissue sections was performed using 4% paraformaldehyde in PBS for 10-20 minutes. Blocking and overnight antibody incubation was performed using 1% normal serum and 2% BSA in PBS followed by exposure to fluorescent conjugated secondary antibody. After counterstaining with Hoechst dye, sections were mounted and imaged. Tumors were classified as follows: low (no expression or less that 10% tumor area), intermediate staining (10-30% tumor area or weak expression throughout the tumor), or high (>30% tumor area). p-p65 staining was classified as negative or positive for each tumor.

Patient radiation response studies

The radiation therapy response was determined by comparing the change in enhancing tumor size between the post-surgical assessment and first post-radiation therapy MRI in previously described manner (Pelloski et al., 2005). Progression was documented by evaluation of serial MRI imaging and dated from the first appearance of progression on MRI, thus minimizing the misclassification of pseudoprogression as true progression. Cases in which progression was not seen in subsequent scans and/or for which subsequent resection failed to identify tumor were deemed pseudoprogression and not counted as progression events. Cases in which only one MRI was available documenting suspected progression were coded as progression. The association of responders/non-responders to IHC expression was performed using Chi Square test. A generalized linear model was constructed using a binomial distribution to determine significant predictors of radiation response (Table S8).

Flow Cytometry

Human GBM patient derived tumor cells as well as human GSCs were dissociated into single cell suspension and stained with primary antibodies against CD133, CD15, and/or CD44 (BD Biosciences), according to manufacturer's instructions. For unconjugated primary antibodies either FITC or PE conjugated secondary antibodies was used after primary antibody incubation. For isotype controls either PE or FITC conjugated immunoglobulins were used. The stained cells were analyzed using a BD LSRII flow cytometer and Fluorescence activated cell sorting (FACS) was performed on a BD Aria II cell sorter (Becton Dickinson). For surgical specimens a fluorescent live cell probe, Calcien-AM (0.4μM, Invitrogen), was added to the staining protocol for cells isolated from fresh specimens to help gate out the cell population from debris in addition to the forward and side scatters.

Cell cycle analysis

GSCs after various treatments were pelleted by centrifugation, and dissociated with Accutase (Sigma) by using a 1 ml sterile pipette. Cells were washed with PBS to remove Accutase and resuspended in 1 ml of cold PBS and fixated with 2 ml of 100% pre-cooled ethanol. After

fixation overnight, cells were resuspended, and washed with FACS buffer (0.5% BSA, 25 mM EDTA in PBS). Cell pellets were then re-suspended in 800 µl of FACS buffer containing 20 µl of RNAse A (10 mg/ml) and incubated at 37^0C for 30 mins. After the incubation period, cells were treated with 50 µl of propidium iodide (500 µg/ml) and cell cycle analysis was performed by using the FACS Calibur flow cytometer (BD Biosciences) followed by analysis by FlowJo (Tree Star Inc.).

γ-H2AX assay

Cells were placed in chamber slides coated with laminin/poly-L-ornithine coated coverslips 24 h prior to treatments. At the indicated timepoints cells were fixed in 4% paraformaldehyde, permeabilized with 0.1% Trixton-X/PBS and stained with γ-H2AX antibody (R&D systems) according to standard protocols. The number of foci formed was counted in at least 25 nuclei for each group.

Apoptosis assay

Apoptosis assay was performed using the Annexin V:PE apoptosis detection kit (BD Biosciences) according to the manufacturer's instructions.

Neurosphere assay

Cells were seeded at 3 cells per well in triplicate 96 well plates (radiation assay) or in equal number in 6 well plates (growth factor assay). For radiation assays, total number of spheres was counted after 3 weeks and control cell sphere number was set to 100% and compared to treatment groups. For growth factor assays, number of spheres (>50 µM) in diameter were counted in five randomly chosen fields and plotted as mean.

DNA, RNA isolation, Real time qRT-PCR and western blotting

Total DNA or RNA from GSCs or formalin fixed, paraffin embedded tumor tissues was prepared using the Masterpure complete DNA and RNA isolation kit (Epicenter) after proteinase K digestion according to the manufacturer's instructions. Inventoried Taqman probes were obtained from Applied Biosystems and qRT-PCR reactions were performed as described previously (Bhat et al., 2011). For western blotting, protein lysis was performed in 0.5% NP-40 lysis buffer and western blot analysis was performed as previously described (Bhat et al., 2011). Antibodies against STAT3, p-STAT3, p-p65 (ser 536, Cell Signaling), p65, YKL-40, C/EBPβ (Santa Cruz Biotechnologies), OLIG2 (IBL), SOX9 (Novus Biologicals), FN1 (BD Biosciences), CD44 (BD Biosciences), TAZ (Novus Biologicals) and actin (Calbiochem) were purchased commercially.

Macrophages/microglia isolation

Glioma derived macrophages/microglia were isolated as previously described (Olah et al., 2012). Briefly, tumor tissue was mechanically disrupted in a glass homogenizer and filtered through 70 µm cell strainer and the resulting cell suspension was centrifuged for 10 min to obtain a cell pellet. The cell pellet was resuspended in Percoll gradient (Percoll 60, 40%, and PBS) and was centrifuged for 20 min at 950 g. The interface consisting of macrophages/microglia was collected, washed, and analyzed by flow cytometery. Cell

suspensions were incubated with human Fc receptor binding inhibitor (eBioscience) to avoid nonspecific staining. The purity of macrophages/microglia was determined by fluorescently labeled primary antibodies directed against CD11b (BioLegend) and CD45 (BioLegend) and the cell viability was determined by DRAQ5 (Biostatus). The surface expression of above mentioned markers was determined by FACS Calibur flow cytometer (Becton Dickinson) and analyzed using WinMDI 2.8 software. Purity was defined as the percentage of DRAQ5 positive cells, showing $CD11b^{high}$ and $CD45^{int}$ expression. Conditioned media was collected from CD11b and CD45 enriched macrophages/microglia plated in 5% serum containing media. After 48-96h of post plating macrophages/microglia conditioned media was collected and filtered through 0.45 μm filters and stored at -80^0C for later experiments.

WST1 assay

Viability of GSCs treated with minocycline was determined using the WST1 assay kit from Clontech. Cells were seeded at 10,000 cells per well in a 96 well plate in at least 3-4 wells with or without minocycline for 5 days after which 10 μl of pre-mixed WST reagent was added per well and absorbance measured at 450 nm after 3 hours.

Primers

Assay type	Assay name	Forward Primer Sequence (5' to 3')	Reverse Primer Sequence (5' to 3')	Probe Oligo Sequence (5' to 3')
CIMP	ANKRD43	TCGTCGGTATCGAGTAGCGG	CGATACTAAACTTCCTACAAAAACACGAC	AATACGCAACTCCGAACTACTAAACCGCTTC
CIMP	HFE	TTTTTGATGTTTTTGTAGATCGCG	CGCGCCCCTAATTCGC	CGAACTCACGCAACAAACGCCCCTA
CIMP	MAL	GTTCGGTGTAGGATTTTAGCGTC	ATCTACAATAAAAAATAAAACCGACCG	CGACCGCCGACCCCTTCCG
CIMP	LGALS3	GCGGAGTTTCGTGGGTTTCG	AATAACCAAACTACGACTCGTCACC	CCGCAAAACGCAAACGACGAAAATACGACG
CIMP	RHOF	GTCGTAGTCGTCGTCGTTTACG	GCTACGAACTCCGAACAATAAATACC	AAACCCTAACCCAAACCGCCGCCC
CIMP	ADPRH	TGTATAGTTCGGGTACGAGAATGTG	TTTAACGTTCGCTTTCAAAACG	TCGTGAAAGTTTAGAGGAGTT
CIMP	COL21A1	CGTTGTAGGGAGAACGGATTTC	CCGAACAAAACCTACGCTAAAAC	CGGAGGGTAGTTAATT
CIMP	HSD11B2	CGCGGTGGTGCGATTAGT	ACATACCACTCACGCTTATTCGAA	AAGGGTATCGGGATGTC
CIMP	RAB27B	GCGGATCGTTCGGTTTTG	CAAAACGATAAACACGAAAACAACTAC	TCGGAGTTATAGGTTGGAGG
CIMP	RILP	GGATCGATAGCGGGACGAAT	CACCGCCTCGATCTCCTAAC	TCGGGCGTATAATC
CIMP	SLITL2	ACGCGGATTCGAACGTAGTT	CCGCGACCTCAATCTTTCC	TCGGGTTCGATTCGT
Reference	COL2A1	TCTAACAATTATAAACTCCAACCACCAA	GGGAAGATGGGATAGAAGGGAATAT	CCTTCATTCTAACCCAATACCTATCCCACCTCTAAA

LOH (Chr. 10) assay	Forward Primer Sequence (5' to 3')	Reverse Primer Sequence (5' to 3')
D10S2472	TCTCCCCACTACATATAACTAAAAACC	GAAGGCACCAATCCATTCAT
D10S2470	TCAAGCTTGCAGACAGCCTA	CATCAAGCATACTGTATTAGTTAGGG
D10S1242	CATGTTTTAACCATCAAGCATACTG	TCAAGCTTGCAGACAGCCTA
D10S541	CATGGAATCTTTTGAAGAACTGG	GGGCCTGCCAGTGAATAGT
D10S2322	CCTGGGAGTAGCAGCAATAG	CCCTCTCCCTACAATGTCCT
D10S1683	TTAAGTGCCAATGCCCAATC	TGCTAACACGACAGTATCCCAGAC

Supplemental References

Abreu, J. G., Ketpura, N. I., Reversade, B., and De Robertis, E. M. (2002). Connective-tissue growth factor (CTGF) modulates cell signalling by BMP and TGF-beta. Nat Cell Biol 4, 599-604.

Bally-Cuif, L., Goridis, C., and Santoni, M. J. (1993). The mouse NCAM gene displays a biphasic expression pattern during neural tube development. Development 117, 543-552.

Bergheim, I., Guo, L., Davis, M. A., Duveau, I., and Arteel, G. E. (2006). Critical role of plasminogen activator inhibitor-1 in cholestatic liver injury and fibrosis. J Pharmacol Exp Ther 316, 592-600.

Bommarito, A., Richiusa, P., Carissimi, E., Pizzolanti, G., Rodolico, V., Zito, G., Criscimanna, A., Di Blasi, F., Pitrone, M., Zerilli, M., et al. (2011). BRAFV600E mutation, TIMP-1 upregulation, and NF-kappaB activation: closing the loop on the papillary thyroid cancer trilogy. Endocr Relat Cancer 18, 669-685.

Caiazzo, M., Dell'Anno, M. T., Dvoretskova, E., Lazarevic, D., Taverna, S., Leo, D., Sotnikova, T. D., Menegon, A., Roncaglia, P., Colciago, G., et al. (2011). Direct generation of functional dopaminergic neurons from mouse and human fibroblasts. Nature 476, 224-227.

Campagnoli, C., Roberts, I. A., Kumar, S., Bennett, P. R., Bellantuono, I., and Fisk, N. M. (2001). Identification of mesenchymal stem/progenitor cells in human first-trimester fetal blood, liver, and bone marrow. Blood 98, 2396-2402.

Capela, A., and Temple, S. (2002). LeX/ssea-1 is expressed by adult mouse CNS stem cells, identifying them as nonependymal. Neuron 35, 865-875.

Casarosa, S., Fode, C., and Guillemot, F. (1999). Mash1 regulates neurogenesis in the ventral telencephalon. Development 126, 525-534.

Cheng, L. C., Pastrana, E., Tavazoie, M., and Doetsch, F. (2009). miR-124 regulates adult neurogenesis in the subventricular zone stem cell niche. Nat Neurosci 12, 399-408.

Cheung, M., and Briscoe, J. (2003). Neural crest development is regulated by the transcription factor Sox9. Development 130, 5681-5693.

D'Amour, K. A., and Gage, F. H. (2003). Genetic and functional differences between multipotent neural and pluripotent embryonic stem cells. Proc Natl Acad Sci U S A 100 Suppl 1, 11866-11872.

Eads, C. A., Danenberg, K. D., Kawakami, K., Saltz, L. B., Blake, C., Shibata, D., Danenberg, P. V., and Laird, P. W. (2000). MethyLight: a high-throughput assay to measure DNA methylation. Nucleic Acids Res *28*, E32.

Eads, C. A., Danenberg, K. D., Kawakami, K., Saltz, L. B., Danenberg, P. V., and Laird, P. W. (1999). CpG island hypermethylation in human colorectal tumors is not associated with DNA methyltransferase overexpression. Cancer Res *59*, 2302-2306.

Eisen, M. B., Spellman, P. T., Brown, P. O., and Botstein, D. (1998). Cluster analysis and display of genome-wide expression patterns. Proc Natl Acad Sci U S A *95*, 14863-14868.

Favaro, R., Valotta, M., Ferri, A. L., Latorre, E., Mariani, J., Giachino, C., Lancini, C., Tosetti, V., Ottolenghi, S., Taylor, V., and Nicolis, S. K. (2009). Hippocampal development and neural stem cell maintenance require Sox2-dependent regulation of Shh. Nat Neurosci 12, 1248-1256.

Ghilzon, R., McCulloch, C. A., and Zohar, R. (1999). Stromal mesenchymal progenitor cells. Leuk Lymphoma 32, 211-221.

Girgrah, N., Ackerley, C. A., and Moscarello, M. A. (1991a). Localization of CD44 (P80) on the external surface of a human astrocytoma cell. Neuroreport 2, 441-444.

Girgrah, N., Letarte, M., Becker, L. E., Cruz, T. F., Theriault, E., and Moscarello, M. A. (1991b). Localization of the CD44 glycoprotein to fibrous astrocytes in normal white matter and to reactive astrocytes in active lesions in multiple sclerosis. J Neuropathol Exp Neurol 50, 779-792.

Hakala, B. E., White, C., and Recklies, A. D. (1993). Human cartilage gp-39, a major secretory product of articular chondrocytes and synovial cells, is a mammalian member of a chitinase protein family. J Biol Chem 268, 25803-25810.

Hashimoto, K., Noshiro, M., Ohno, S., Kawamoto, T., Satakeda, H., Akagawa, Y., Nakashima, K., Okimura, A., Ishida, H., Okamoto, T., et al. (1997). Characterization of a cartilage-derived 66-kDa protein (RGD-CAP/beta ig-h3) that binds to collagen. Biochim Biophys Acta 1355, 303-314.

Haudenschild, D. R., McPherson, J. M., Tubo, R., and Binette, F. (2001). Differential expression of multiple genes during articular chondrocyte redifferentiation. Anat Rec 263, 91-98.

Hennen, E., Czopka, T., and Faissner, A. (2011). Structurally distinct LewisX glycans distinguish subpopulations of neural stem/progenitor cells. J Biol Chem 286, 16321-16331.

Kang, P., Lee, H. K., Glasgow, S. M., Finley, M., Donti, T., Gaber, Z. B., Graham, B. H., Foster, A. E., Novitch, B. G., Gronostajski, R. M., and Deneen, B. (2012). Sox9 and NFIA coordinate a transcriptional regulatory cascade during the initiation of gliogenesis. Neuron 74, 79-94.

Kuppner, M. C., Van Meir, E., Gauthier, T., Hamou, M. F., and de Tribolet, N. (1992). Differential expression of the CD44 molecule in human brain tumours. Int J Cancer 50, 572-577.

Kusumi, K., Dunwoodie, S. L., and Krumlauf, R. (2001). Dynamic expression patterns of the pudgy/spondylocostal dysostosis gene Dll3 in the developing nervous system. Mech Dev 100, 141-144.

Kusumi, K., Mimoto, M. S., Covello, K. L., Beddington, R. S., Krumlauf, R., and Dunwoodie, S. L. (2004). Dll3 pudgy mutation differentially disrupts dynamic expression of somite genes. Genesis 39, 115-121.

Kuvaja, P., Hulkkonen, S., Pasanen, I., Soini, Y., Lehtonen, S., Talvensaari-Mattila, A., Paakko, P., Kaakinen, M., Autio-Harmainen, H., Hurskainen, T., et al. (2012). Tumor tissue inhibitor of metalloproteinases-1 (TIMP-1) in hormone-independent breast cancer might originate in stromal cells, and improves stratification of prognosis together with nodal status. Exp Cell Res 318, 1094-1103.

Leask, A. (2004). Transcriptional profiling of the scleroderma fibroblast reveals a potential role for connective tissue growth factor (CTGF) in pathological fibrosis. Keio J Med 53, 74-77.

Lee, C. G., Hartl, D., Lee, G. R., Koller, B., Matsuura, H., Da Silva, C. A., Sohn, M. H., Cohn, L., Homer, R. J., Kozhich, A. A., et al. (2009). Role of breast regression protein 39 (BRP-39)/chitinase 3-like-1 in Th2 and IL-13-induced tissue responses and apoptosis. J Exp Med 206, 1149-1166.

Lu, Q. R., Sun, T., Zhu, Z., Ma, N., Garcia, M., Stiles, C. D., and Rowitch, D. H. (2002). Common developmental requirement for Olig function indicates a motor neuron/oligodendrocyte connection. Cell 109, 75-86.

Lu, Q. R., Yuk, D., Alberta, J. A., Zhu, Z., Pawlitzky, I., Chan, J., McMahon, A. P., Stiles, C. D., and Rowitch, D. H. (2000). Sonic hedgehog--regulated oligodendrocyte lineage genes encoding bHLH proteins in the mammalian central nervous system. Neuron 25, 317-329.

Madhavan, S., Zenklusen. J.C., Kotliarov,Y., Sahni, H., Fine, H.A., Buetow, K. (2009). Rembrandt: helping personalized medicine become a reality through integrative translational research. Mol Cancer Res. 7: 157-167.

Mao, Y., and Schwarzbauer, J. E. (2005). Fibronectin fibrillogenesis, a cell-mediated matrix assembly process. Matrix Biol 24, 389-399.

Mayer-Proschel, M., Kalyani, A. J., Mujtaba, T., and Rao, M. S. (1997). Isolation of lineage-restricted neuronal precursors from multipotent neuroepithelial stem cells. Neuron 19, 773-785.

Mayrand, D., Laforce-Lavoie, A., Larochelle, S., Langlois, A., Genest, H., Roy, M., and Moulin, V. J. (2012). Angiogenic properties of myofibroblasts isolated from normal human skin wounds. Angiogenesis 15, 199-212.

Mosher, D. F. (1984). Physiology of fibronectin. Annu Rev Med 35, 561-575.

Nakanishi, T., Nishida, T., Shimo, T., Kobayashi, K., Kubo, T., Tamatani, T., Tezuka, K., and Takigawa, M. (2000). Effects of CTGF/Hcs24, a product of a hypertrophic chondrocyte-specific gene, on the proliferation and differentiation of chondrocytes in culture. Endocrinology 141, 264-273.

Narumoto, O., Matsuo, Y., Sakaguchi, M., Shoji, S., Yamashita, N., Schubert, D., Abe, K., Horiguchi, K., and Nagase, T. (2012). Suppressive effects of a pyrazole derivative of curcumin on airway inflammation and remodeling. Exp Mol Pathol 93, 18-25.

Ohno, S., Doi, T., Tsutsumi, S., Okada, Y., Yoneno, K., Kato, Y., and Tanne, K. (2002). RGD-CAP ((beta)ig-h3) is expressed in precartilage condensation and in prehypertrophic chondrocytes during cartilage development. Biochim Biophys Acta 1572, 114-122.

Olah, M., Raj, D., Brouwer, N., De Haas, A. H., Eggen, B. J., Den Dunnen, W. F., Biber, K. P., and Boddeke, H. W. (2012). An optimized protocol for the acute isolation of human microglia from autopsy brain samples. Glia *60*, 96-111.

Ostanin, A. A., Petrovskii, Y. L., Shevela, E. Y., and Chernykh, E. R. (2011). Multiplex analysis of cytokines, chemokines, growth factors, MMP-9 and TIMP-1 produced by human bone marrow, adipose tissue, and placental mesenchymal stromal cells. Bull Exp Biol Med 151, 133-141.

Parras, C. M., Hunt, C., Sugimori, M., Nakafuku, M., Rowitch, D., and Guillemot, F. (2007). The proneural gene Mash1 specifies an early population of telencephalic oligodendrocytes. J Neurosci 27, 4233-4242.

Parsons, D. W., Jones, S., Zhang, X., Lin, J. C., Leary, R. J., Angenendt, P., Mankoo, P., Carter, H., Siu, I. M., Gallia, G. L.*, et al.* (2008). An integrated genomic analysis of human glioblastoma multiforme. Science *321*, 1807-1812.

Pennartz, S., Belvindrah, R., Tomiuk, S., Zimmer, C., Hofmann, K., Conradt, M., Bosio, A., and Cremer, H. (2004). Purification of neuronal precursors from the adult mouse brain: comprehensive gene expression analysis provides new insights into the control of cell migration, differentiation, and homeostasis. Mol Cell Neurosci 25, 692-706.

Pruszak, J., Ludwig, W., Blak, A., Alavian, K., and Isacson, O. (2009). CD15, CD24, and CD29 define a surface biomarker code for neural lineage differentiation of stem cells. Stem Cells 27, 2928-2940.

Read, T. A., Fogarty, M. P., Markant, S. L., McLendon, R. E., Wei, Z., Ellison, D. W., Febbo, P. G., and Wechsler-Reya, R. J. (2009). Identification of CD15 as a marker for tumor-propagating cells in a mouse model of medulloblastoma. Cancer Cell 15, 135-147.

Ross, S. E., Greenberg, M. E., and Stiles, C. D. (2003). Basic helix-loop-helix factors in cortical development. Neuron 39, 13-25.

Samarakoon, R., Overstreet, J. M., Higgins, S. P., and Higgins, P. J. (2012). TGF-beta1 --> SMAD/p53/USF2 --> PAI-1 transcriptional axis in ureteral obstruction-induced renal fibrosis. Cell Tissue Res 347, 117-128.

Scott, C. E., Wynn, S. L., Sesay, A., Cruz, C., Cheung, M., Gomez Gaviro, M. V., Booth, S., Gao, B., Cheah, K. S., Lovell-Badge, R., and Briscoe, J. (2010). SOX9 induces and maintains neural stem cells. Nat Neurosci 13, 1181-1189.

Stolt, C. C., Lommes, P., Sock, E., Chaboissier, M. C., Schedl, A., and Wegner, M. (2003). The Sox9 transcription factor determines glial fate choice in the developing spinal cord. Genes Dev 17, 1677-1689.

Stolt, C. C., Rehberg, S., Ader, M., Lommes, P., Riethmacher, D., Schachner, M., Bartsch, U., and Wegner, M. (2002). Terminal differentiation of myelin-forming oligodendrocytes depends on the transcription factor Sox10. Genes Dev 16, 165-170.

Sugiura, Y., Ma, L., Sun, B., Shimada, H., Laug, W. E., Seeger, R. C., and DeClerck, Y. A. (1999). The plasminogen-plasminogen activator (PA) system in neuroblastoma: role of PA inhibitor-1 in metastasis. Cancer Res 59, 1327-1336.

Sun, S., Guo, Z., Xiao, X., Liu, B., Liu, X., Tang, P. H., and Mao, N. (2003). Isolation of mouse marrow mesenchymal progenitors by a novel and reliable method. Stem Cells 21, 527-535.

Takebayashi, H., Nabeshima, Y., Yoshida, S., Chisaka, O., and Ikenaka, K. (2002). The basic helix-loop-helix factor olig2 is essential for the development of motoneuron and oligodendrocyte lineages. Curr Biol 12, 1157-1163.

Taranova, O. V., Magness, S. T., Fagan, B. M., Wu, Y., Surzenko, N., Hutton, S. R., and Pevny, L. H. (2006). SOX2 is a dose-dependent regulator of retinal neural progenitor competence. Genes Dev 20, 1187-1202.

TCGA. (2008) Comprehensive genomic characterization defines human glioblastoma genes and core pathways. Nature 455, 1061-1068.

Thiery, J. P., Duband, J. L., Rutishauser, U., and Edelman, G. M. (1982). Cell adhesion molecules in early chicken embryogenesis. Proc Natl Acad Sci U S A 79, 6737-6741.

Ueno, T., Ito, J., Hoshikawa, S., Ohori, Y., Fujiwara, S., Yamamoto, S., Ohtsuka, T., Kageyama, R., Akai, M., Nakamura, K., and Ogata, T. (2012). The identification of transcriptional targets of Ascl1 in oligodendrocyte development. Glia 60, 1495-1505.

Wegner, M., and Stolt, C. C. (2005). From stem cells to neurons and glia: a Soxist's view of neural development. Trends Neurosci 28, 583-588.

Yoon, K., and Gaiano, N. (2005). Notch signaling in the mammalian central nervous system: insights from mouse mutants. Nat Neurosci 8, 709-715.

Yuan, S. H., Martin, J., Elia, J., Flippin, J., Paramban, R. I., Hefferan, M. P., Vidal, J. G., Mu, Y., Killian, R. L., Israel, M. A., et al. (2011). Cell-surface marker signatures for the isolation of neural stem cells, glia and neurons derived from human pluripotent stem cells. PLoS One 6, e17540.

Zhao, X., D, D. A., Lim, W. K., Brahmachary, M., Carro, M. S., Ludwig, T., Cardo, C. C., Guillemot, F., Aldape, K., Califano, A., et al. (2009). The N-Myc-DLL3 cascade is suppressed by the ubiquitin ligase Huwe1 to inhibit proliferation and promote neurogenesis in the developing brain. Dev Cell 17, 210-221.

Zhou, Q., and Anderson, D. J. (2002). The bHLH transcription factors OLIG2 and OLIG1 couple neuronal and glial subtype specification. Cell 109, 61-73.

Zhou, Q., Wang, S., and Anderson, D. J. (2000). Identification of a novel family of oligodendrocyte lineage-specific basic helix-loop-helix transcription factors. Neuron 25, 331-343.

Zohar, R., Cheifetz, S., McCulloch, C. A., and Sodek, J. (1998). Analysis of intracellular osteopontin as a marker of osteoblastic cell differentiation and mesenchymal cell migration. Eur J Oral Sci 106 Suppl 1, 401-407.